

## Trabajo Fin de Máster

Sistema de estimulación extracelular para la modificación de parámetros de red en redes neuronales en cultivo

Extracellular stimulation system for the modification of network parameters in cultured neural networks

Autor/es

Leonardo Daniel Garma Gavira

Director/es

Michele Fiscella  
Pablo Laguna Lasaosa (Ponente)



## DECLARACIÓN DE AUTORÍA Y ORIGINALIDAD

(Este documento debe acompañar al Trabajo Fin de Grado (TFG)/Trabajo Fin de Máster (TFM) cuando sea depositado para su evaluación).

D./D<sup>a</sup>. LEONARDO GARMA GAVIRA,

con nº de DNI 05300772P en aplicación de lo dispuesto en el art.

14 (Derechos de autor) del Acuerdo de 11 de septiembre de 2014, del Consejo

de Gobierno, por el que se aprueba el Reglamento de los TFG y TFM de la

Universidad de Zaragoza,

Declaro que el presente Trabajo de Fin de (Grado/Máster)

Máster \_\_\_\_\_, (Título del Trabajo)

EXTRACELLULAR STIMULATION SYSTEM FOR THE MODIFICATION OF NETWORK  
PARAMETERS IN CULTURED NEURAL NETWORKS

es de mi autoría y es original, no habiéndose utilizado fuente sin ser citada  
debidamente.

Zaragoza, 29 de Agosto de 2017

Fdo: \_\_\_\_\_



## Resumen

Este proyecto se centra en el uso de dispositivos de microelectrodos MEAs (Multi Electrode Arrays) de última generación para el estudio y la manipulación de redes neuronales en cultivo. Chips MEA, con 26400 electrodos situados en una superficie de  $3.85 \times 2.10 \text{ mm}^2$ , fueron utilizados para registrar la actividad eléctrica de dos cultivos de neuronas corticales disociadas obtenidas de embriones de rata. En las mismas plataformas MEA, se implementó un protocolo de estimulación en bucle cerrado, de manera que se pudieran enviar pulsos eléctricos de estimulación a determinados electrodos en respuesta a potenciales de acción detectados en otro electrodo. Uno de los cultivos de neuronas fue sometido al protocolo de estimulación en bucle cerrado mientras que el segundo cultivo fue utilizado como control. Se desarrollaron diferentes métodos con el fin de hacer una caracterización funcional de los cultivos. El análisis funcional de los registros obtenidos en los experimentos indican que la estimulación en bucle cerrado provocó pérdidas significativas y generalizadas de actividad y conectividad en la red neuronal en cultivo.

## Abstract

This project focuses on the use of a state of the art microelectrode array (MEAs) chip for the study and manipulation of cultured neural networks. MEA chips containing 26400 electrodes arranged on a sensing area of  $3.85 \times 2.10 \text{ mm}^2$  were used to obtain electrical recordings from two cultures of dissociated cortical neurons from pre-natal rats. A closed-loop stimulation protocol was implemented on the MEA platforms so that stimulation pulses could be delivered to a determined electrode on the array in response to action potentials detected on another electrode. One of the neuronal cultures was subjected to a closed-loop stimulation protocol whereas the second one was used as a control. Several different metrics were implemented and applied to the recordings in order to perform a functional characterization of the cultures. The functional analysis of the recordings obtained in the stimulation experiments indicates that the closed-loop stimulation induced a significant and generalized loss of activity and connectivity in the cultured neuronal network.

## Acknowledgments

This work was carried out in its entirety at the Bio Engineering Laboratory (BEL) at the Department of Biosystems Science and Engineering from the Swiss Federal Institute of Technology in Zürich, Switzerland.

I am deeply grateful to my supervisors, Dr. Michele Fiscella and Dr. Jan Müller for giving the opportunity to participate in this project and for their guidance and supervision. This work would not have been possible without their involvement, I am truly thankful to them for providing me with such an enriching learning experience. I would also like to express my deepest gratitude to Professor Andreas Hierlemann for allowing me to work in his research group and for providing financial support for this project. I would also like to acknowledge Professor Pablo Laguna Lasao and Dr. M<sup>a</sup> Ángeles Pérez Ansón for their feedback and support toward the completion of this project.

I am thankful to all the members of the BEL for their invaluable help and advice and the many fruitful discussions. In particular grateful to Dr. Felix Franke, Dr. Sydney Geissler, Roland Diggelmann, Wei Gong, Dr. Manuel Schröter, Dr. Sergey Sitnikov and Dr. Marie Obien. Their knowledge and expertise played a critical role in the completion of this work. I would also like to thank Brigitta Elhadj for all her help in all official matters. Finally I would like to express my gratitude to Jonas De Tribolet for his feedback and help toward the completion of this work.

# Contents

<b>1</b>	<b>Introduction</b>	<b>6</b>
1.1	Overview . . . . .	6
1.2	Motivation . . . . .	6
1.3	Electrophysiological study of neural networks . . . . .	7
1.3.1	Electrophysiological techniques . . . . .	8
1.3.2	MEAs for in vitro studies . . . . .	9
1.3.3	In vitro studies of neural networks . . . . .	11
<b>2</b>	<b>Methods</b>	<b>13</b>
2.1	MEAs . . . . .	13
2.2	Cell cultures . . . . .	14
2.3	Electrode selection . . . . .	15
2.4	Spike Sorting . . . . .	16
2.4.1	Quality assessment . . . . .	18
2.5	Characterization . . . . .	18
2.5.1	Basic features . . . . .	18
2.5.2	Bursting behavior . . . . .	18
2.5.3	Connectivity . . . . .	19
2.5.4	Network properties . . . . .	19
2.6	Closed-loop Stimulation . . . . .	20
<b>3</b>	<b>Results</b>	<b>22</b>
3.1	Deviation-based electrode selection improves over current methods	22
3.2	Automated spike sorting obtains poor results from cortical cultures recordings . . . . .	31
3.3	Implementation of Closed-loop Stimulation . . . . .	36
3.4	Effects of Closed-loop Stimulation . . . . .	36
3.4.1	Closed-loop stimulation causes loss of activity and reduction of AP amplitudes . . . . .	37
3.4.2	Bursting patterns . . . . .	38
3.4.3	Bursts features . . . . .	40
3.4.4	Closed-loop stimulation causes loss of connectivity . . . . .	42
<b>4</b>	<b>Discussion</b>	<b>46</b>
<b>5</b>	<b>Conclusion</b>	<b>49</b>
	<b>References</b>	<b>50</b>
<b>6</b>	<b>ANNEXES</b>	<b>58</b>
6.1	Annex I . . . . .	59
6.2	Annex II . . . . .	65

# 1 Introduction

The goal of this project was to implement and study the effects of a closed-loop stimulation protocol on cultured neural networks, with the aim of developing a methodology capable of inducing reproducible modifications of the network parameters. More broadly, the project made use of state of the art microelectrode array (MEA) chips to monitor and analyze the activity of neural networks developed in vitro. The same MEA chips were then used to automatically deliver stimulation pulses in response to the network's activity (closed-loop stimulation).

The project builds upon the successful implementation and use of closed-loop stimulation protocols on earlier versions of the MEA chips [1] and represents an innovative approach in its scope, trying to analyze and modify the behavior of the neuronal culture at the network level rather than focusing on single pairs of cells.

## 1.1 Overview

The thesis is organized as follows: The rest of this section provides an introduction to the electrophysiological study of neurons, the study of neural networks in vitro and the MEAs technology. The methods section describes in detail the approach taken in the development of this work, specifying how the neurons were obtained and cultured, how the recordings were performed, which techniques were employed to examine and characterize the neuronal cultures, how the stimulation protocol was implemented and the imaging technique used to observe the networks. The results section describes the outcome of the experiments. The discussion section provides insight on the results, proposing explanations for the observations and suggesting future experiments. Finally, the conclusion section summarizes the outcome of the study.

## 1.2 Motivation

The impairment of neuronal function at the cellular or network levels is linked to a wide range of disorders and diseases. For instance, epilepsy is associated with a specific behavior of the neurons in which they produce repetitive synchronous electrical discharges (bursting) [2]; defects in synaptic transmission [3, 4] and altered balances in the number or strength of inhibitory and excitatory synapses [5, 6, 7, 8] have been identified as a possible causes of autism spectrum disorders; and Parkinson's disease has been related to an impairment of midbrain dopamine neurons to synthesize and release dopamine [9].

The use of MEAs for the analysis and stimulation of neural cultures in disease models has already shown promising results in the understanding and treatment some neurological disorders [10, 11]. In particular, closed-loop stimulation protocols applied through MEAs has proven effective in neurorehabilitation [12] and to mitigate epileptic seizures [13, 11, 14] and Parkinsonism [15]. Additionally, MEAs are an excellent system for drug discovery and basic neuroscience



research [16, 17, 18] and are a key component for state of the art brain-machine interfaces [19, 20], including their clinical applications [21, 22]. The advent of new MEA platforms with unprecedented electrode density [23, 24] can push such applications further by providing the ability to both observe and stimulate neurons at multiple scales, from sub-cellular to network levels. It is therefore imperative to develop and establish methodologies that take advantage of these new platforms to study and modify in vitro neuronal cultures.

### **1.3 Electrophysiological study of neural networks**

Neurons are a highly specialized cell type found in the nervous system of all vertebrates and most invertebrates. In the human brain, neurons are responsible for information processing and transmission. The physiology of neurons allows them to achieve these tasks through a combination of chemical and electrical mechanisms, which are used by the cells to form intricate communication networks [25].

The physiology of human neurons is rather diverse, as they can be classified into several types according to their structure. However, they all present a cell body which contains the nucleus (soma) and a several protrusions (neurites) that can be classified as axons and dendrites. Axons are elongated extensions of the cell body which behave as highly efficient conducts for electrical signals whereas dendrites are extensions that connect to the axons of other cells forming synapses [26]. The presence of voltage-triggered ion channels allows neurons to maintain a differential electrical potential across their membranes. This potential changes as a function of the concentrations of ions on both sides of the membrane, which can be modified by the cell in response to incoming chemical or electrical signals. Either as a result of the integration of these incoming signals or as a spontaneous process, neurons can generate a specific type of electrical pulse known as action potential (AP). The AP consists of a strong and rapid drop followed by a sudden increase in the cell membrane potential that is propagated along the axon. The shape of the AP is caused by a determined sequence of activation and inactivation of different ion channels (Figure 1) [27].

Action potentials, also referred to as spikes, are one of the main mechanisms used by neurons to communicate with one another. Therefore, monitoring the membrane potentials to detect spikes is key to understanding how information is being transmitted and processed in neural networks.

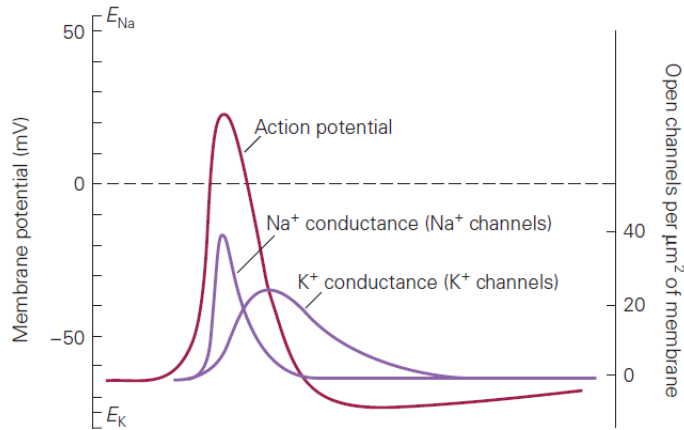


Figure 1: Hodgkin-Huxley model of action potential. The purple lines show the conductance of  $\text{Na}^+$  and  $\text{K}^+$  ions, expressed in number of channels. The membrane potential resulting from the conductance of these two ions in the model is shown in red. The shape of the AP appears as a result of the sequential opening of voltage-gated  $\text{Na}^+$  and  $\text{K}^+$  channels. Reproduced from [27]

### 1.3.1 Electrophysiological techniques

There are different techniques in which electrodes can be used to observe the membrane potentials. Depending on the location of the electrodes with respect to the cell, these techniques can be classified into three groups: intracellular recordings, in which the electrode is placed inside the cell, patch clamp recordings, in which the electrode is placed adjacent to the cell membrane, and extracellular recordings, in which the electrode is nearby the cell. Although intracellular and patch clamp recordings provide the most direct and precise measures, they are technically challenging and limited in scope. The electrodes are placed in glass micropipettes that need to be manually placed in the desired location (with the help of microscopes and micromanipulators), allowing to act on a single cell at a time. Additionally, these techniques are harmful to the cells, and thus neurons survive only for a few hours after the electrodes is inserted [28].

On the other hand, extracellular recordings [29] provide less accurate measures of the membrane potential but offer dramatic technical advantages. The electrodes do not need to be positioned so precisely and the procedure does not damage the cells, working through a non-invasive contact with the cell membrane that allows long-term recordings. Thus instead of a single micropipette, it is also possible to use arrays of microelectrodes to perform these recordings, providing information on ensembles of neurons rather than on a single one. Therefore, extensive work has been done on the development of techniques for the fabrication of multi-electrode arrays, moving from stereodes [30] to tetrodes [31, 32], multi-channel platforms [33] and finally high density microelectrode

arrays [23, 24], with the number of simultaneously recorded neurons growing exponentially over the past few decades[34]. These platforms have been extensively used for a variety of applications both in vivo [35, 36, 37, 38, 39, 21] and in vitro [40, 41, 42, 43, 44, 45].

### 1.3.2 MEAs for in vitro studies

Using planar MEAs coated with cell-adhesion substrates, it is possible to cultivate neurons directly on top of the arrays. The transmembrane ion currents cause changes in the extracellular electric fields which are detected as the potential difference between the plasma membrane and the extracellular reference electrode. The level of the potential varies depending on the distance from the cell to the recording site and magnitude of the transmembrane current [18, 46]. The principles of the planar electrodes recordings are presented schematically in Figure 2.

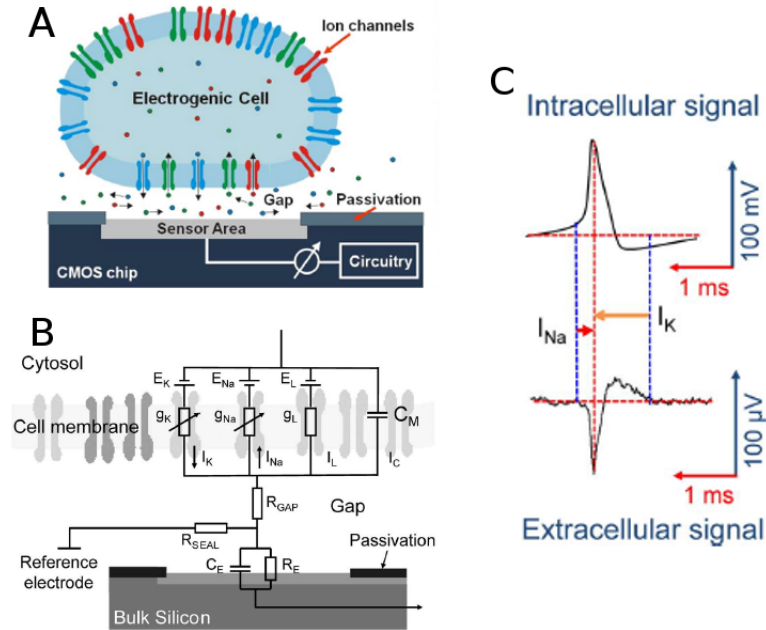


Figure 2: A) Schematic of a cell attached to a sensor surface. A cell featuring ion channels sits on a planar microsensor. Moving ions in the electrode vicinity generate an electric field or voltage that is recorded by the microsensor. B) Electrical equivalent circuit of a membrane adjacent to a sensor. The equivalent model relies on the Hodgkin-Huxley model of the squid axon [27]. The electrode is represented by a capacitor and a resistor in parallel. C) Intracellular neuronal signal recorded by using the patch-clamp technique and an extracellular signal recorded by means of a metal electrode. Reproduced from [46].

The design challenge in this type of arrays is to offer a high electrode density, (so that it is possible to monitor an increasing number of cells at sub-cellular resolution) while providing a high signal-to-noise ratio (SNR). Passive MEAs, which typically consist of metal electrodes on a glass substrate, are limited in both the number of electrodes (usually less than 300) and the spatial resolution (typically  $30 \geq \mu m$ ) [24]. The use of complementary metal-oxide-semi-conductor (CMOS) technology enables the increase of the electrode count, from dozens to tens of thousands of electrodes, dramatically enhancing the spatial resolution. The MEAs that take advantage of this technology have a high electrode density and are referred to as HD-MEAs [46].

In order to increase the SNR, it is necessary to use amplifiers which are larger than the area covered by an electrode. The amplifiers have to be placed on-chip, since placing the electrodes off-chip introduces parasitic signals and interferences. As a result, the chips contain less amplifiers (and therefore readout channels) than electrodes. This approach presents a connectivity challenge, since not all electrodes can be connected to amplifiers at the same time and it is necessary to route a subset of them to the readout channels. CMOS technology allows the implementation of transistors under the electrodes. These transistor can act as switches that can be used to route the signal from a selected group of electrodes to the amplifiers, implementing what is known as a switch matrix [47] and solving the connectivity problem.

The current alternative to these approaches are active pixel sensor (APS) MEAs [48, 49, 50]. These arrays work in a manner similar to image sensors used in cameras, allowing all electrodes to be sampled at fast speeds in full-frame readout. This offers great spatial resolution, however it imposes a limit on the size of the amplifiers, which consequently reduces the SNR and therefore limits the size of the signals that can be distinguished from noise.

The “MEA1K” chip developed at the BEL [23, 24] consist of MEA that makes use of both the CMOS and switch matrix technologies and a printed circuit board (PCB) which provides connectivity to the array. The microelectrode array has 26,400 electrodes at a pitch of  $17.5\mu m$ , covering an area of  $3.85 \times 2.1 mm^2$ . It has 1024 readout channels, which can also be used as stimulation channels to deliver electrical pulses. The electrodes are sampled with 10-bit resolution at a rate of 20kHz, so that when all 1024 channels are routed to electrodes the chip outputs 24MB of data per second.

A second PCB (MEA board) provides power to the circuitry on the chip and acts a bridge between the chip and a FPGA board. The FPGA itself acts as the interface between a host computer and the MEA board. The FPGA provides bi-directional communication: on one side it acquires the raw data data coming from the board and sends it to the host computer and, on the other, it sends the configuration commands for the electrode routing from the host computer to the board. The MEA1K chip, together with the MEA board and the FPGA board conform a complete system capable of obtaining extracellular recordings from cultures placed on top of the chip.

### 1.3.3 In vitro studies of neural networks

Using HD-MEAs, it is possible to record signals from virtually all the neurons in a cultured network. However, the analysis of such signals allowing to reconstruct and understand the functional network existing in the culture is not trivial and presents a number of technical challenges [51]. First, it is necessary to detect and classify the detected APs or spikes (assigning each to a neuron), in a process known as spike sorting [52]. Secondly, the firing regimes of the neurons need to be analyzed. The behavior of neurons can be separated into tonic firing and bursts. In the first one, the neuron fires well spaced spikes, so that the resting potential is reached after each one. During bursts, the neuron fires repeatedly, reducing the interval between APs and exhibiting altered waveforms (usually showing a progressive decrease in amplitude) [53]. Bursts also happen as network-wide events, that is, network bursts, during which most of the neurons in the culture fire with a very high frequency. The detection and analysis of these events has been shown to be very relevant for characterizing in vitro neural networks [45, 54]. Lastly, it is necessary to study the relationships between the sequences of spikes (called “spike trains”) from the different neurons to understand the connectivity between the cells [55].

None of the steps in this analytic process has a fully established methodology yet. The detection of spike events is usually done using a threshold-based method. However it has been disputed whether if this method is reliable when applied to superimposed signals from multiple neurons (as it happens in HD-MEAs) [52]. Neurons present dynamic behaviors, with non-stationary waveforms that change in shape and size, which makes the spike classification a complex task. Moreover, the large volumes of data obtained from HDMEAs and the number of cells present of a cultured network, make it hardly feasible to have a manual classification. Therefore, a large number of different methods using different approaches have been developed for the automatic classification of spikes [56, 57, 58, 59].

The definition of what constitutes a burst or a network bursts in a recording are not entirely settled. Thus, also a number of different methods have been developed for burst detection. They are mainly based on either the analysis of inter-spike intervals of single neurons or on the frequency of spike events in whole populations [60, 61, 54, 62]. Similarly, it is not yet resolved how to compute the functional connectivity in a neural network based on MEAs recordings. Some methods propose the use of different correlation metrics [55, 63], whereas others have proposed the use of information-theoretic metrics such as the transfer entropy [64, 65]. Lacking a ground-truth for the connectivity of large ensembles of neurons, it is still hard to discard any of the proposed methods.

Despite the lack of standardized analysis methods and the diversity of the available MEAs, already a myriad of successful studies have been performed using microelectrode arrays to analyze different aspects of cultured neural networks: from electrical identification and stimulation of sub-cellular compartments [66], to the analysis of network-theoretic properties of neural networks

[67], memory and plasticity [68] or the characterization of developmental stages [45]. Therefore the MEA technology has already demonstrated to be mature and useful for the study of neural networks in vitro.

## 2 Methods

In the development of this project, two sets of pre-natal rat dissociated neurons were plated on MEA1K chips. These neurons were cultured and monitored for activity throughout their development. At 22 days in vitro (DIV), one of the cultures was subjected to a closed-loop stimulation protocol, delivered through the same chip in which they it was grown. The second culture was used as a control to monitor the magnitude of the spontaneous changes. The same stimulation protocol was repeated at 26 DIV. Both at 22 and at 26 DIV, three recordings were obtained from each culture: an initial recording to use as baseline, a second recording done after one hour to use as a blank and reveal the spontaneous short-term changes, and a third recording done after the application of the stimulation.

### 2.1 MEAs

The recording and stimulation of neurons was performed using two MEA1K chips as part of an extracellular recording setup. The chips have a total of 26,400 electrodes of which 1024 can be connected to readout channels simultaneously. The routing that connects a set of electrodes to a set of readout channels is referred to as a configuration.

The electrodes can be directly exposed to the cells and the cell culture media, however, the rest of the chip needs to be protected from having contact with the liquids used in the cell culture process. In order to do so, the area around the electrode array is covered with epoxy in a process called packaging. The cells plated on top of the electrodes need to be covered with media, thus a glass ring was placed around the electrode array, allowing to accommodate a volume of ~2ml. The chips before and after the packaging process are shown in Figure 3. The full packaging protocol is presented in detail in Annex I (6.1).

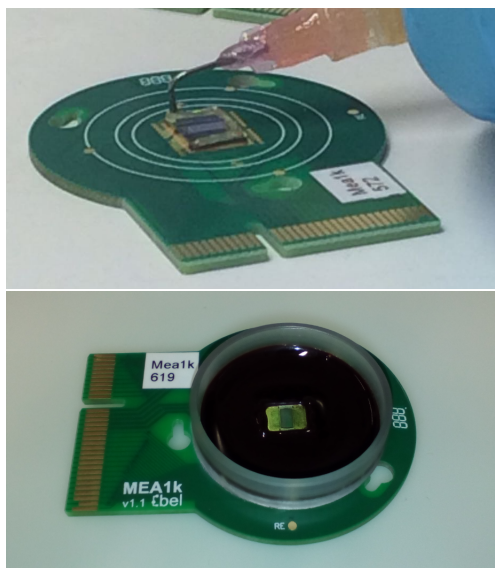


Figure 3: MEA1K chip before (top) and after (bottom) packaging.

## 2.2 Cell cultures

Cortical neurons were obtained from Wistar rat embryos (at embryonic day 18, E18). A total of 6 embryos were first surgically removed from a pregnant rat. The brains were dissected, isolating the cortices which were then dissociated enzymatically in trypsin followed by mechanical trituration. After removing the debris and resuspending the cells in plating media (Neurobasal supplemented with 10% horse serum), the concentration of cells was estimated using a hemocytometer under the microscope.

To ensure the adhesion of the neurons to the surface of the electrode arrays and to improve the survival of the cultures, the electrode arrays were cleaned with ethanol and then treated with polyethylenimine (PEI) and laminin. After cleaning them with ethanol and letting them dry, the electrodes were covered with  $100\mu\text{l}$  of PEI to increase the hydrophobicity of the surface. After 60 minutes, the PEI droplet was removed with an aspirator and the electrodes were washed three times with 1ml of sterile water. Then a droplet of  $10\mu\text{l}$  of laminin was added on top of the center of the array, to increase cell adhesion. The laminin was incubated for 20 minutes at 37 degrees and then partially removed. Afterwards, 40000 cells were plated by placing a droplet of the cell suspension on top of the electrodes. The plated chips were placed in the incubator at 37 degrees in order to allow the cells to attach to the laminin. Subsequently, 1ml of plating media was added. After two days, the plating media was replaced by Dulbecco's Modified Eagle's Medium (DMEM) with 10% horse serum. The DMEM media was kept fresh by replacing half of its volume twice a week.



### 2.3 Electrode selection

The MEA1K chip contains a total of 26400 electrodes, however it is only possible to record from a total of 1024 of them. In order to maximize the amount of information about the neuronal networks cultured on top of the chips, it was necessary to decide which subset of electrodes to record from. In order to do so, the whole array was scanned by making 1 minute recordings of different configurations, so that in the end a one-minute recording from each electrode was available. These short recordings provided information that was used to decide which electrodes were most suitable ones.

The recordings from the scan were filtered using a band-pass filter to isolate the frequencies between 300 and 7000 kHz. APs were detected using the MATLAB peak detection function. On each channel, the peaks larger than 5.5 times the standard deviation of the signal were considered as valid APs. The peaks were required to be spaced, so after a detection the peaks in the next 20 samples were ignored. The 10 samples prior to the APs and the 20 samples after them were stored as the waveforms associated with the AP.

Based on the detected APs, four features were computed for each electrode: firing rate, average peak amplitude, peak amplitude deviation and waveform deviation. The firing rate was calculated as the total number of APs detected divided by the recording time in seconds. The peak amplitude deviation was meant to reflect the variation in the AP amplitude caused by the cells that generate them. This measure was intended to discriminate between electrodes whose signal source was a single cell and those that were recording signals from multiple neurons. The deviation in the amplitude of the detected peaks can be described as the sum of three components:

$$\sigma_A = \sigma_N + \sigma_C + \sigma_J, \quad (1)$$

where  $\sigma_N$  is the deviation due to the random noise of the signal,  $\sigma_C$  is the deviation associated to the cell and  $\sigma_J$  is the deviation caused by the jitter. Taking the assumption that the high sampling frequency would make  $\sigma_J$  insignificant in comparison with the other two sources of deviation and that  $\sigma_N$  can be estimated by the standard deviation of the signal,  $\sigma_C$  can be estimated as

$$\sigma_C = \sigma_A - \sigma_N. \quad (2)$$

Since the deviation in the peak amplitude is expected to be proportional to the magnitude of the peak amplitude (i.e. larger peaks are expected to produce larger deviations), the  $\sigma_C$  values from each electrode were divided by the average amplitude of the peaks observed in the same electrode. The waveform deviation was computed as the mean standard deviation of the whole waveform for all the waveforms collected on each electrode.

Having computed these four features, the electrode selection was done in three steps: first, the electrodes with the 10% largest amplitudes and activity above 2 peaks per second were chosen and the rest discarded. Then, the electrodes on this

initial selection were then ranked according to the harmonic average of their deviation in peak amplitude and waveform deviation. The first 1024 electrodes on the ranking were used as an initial selection. Finally, the selection was populated to ensure that no isolated electrodes were present. Whenever an electrode was found to have less than 2 neighboring electrodes also included in the selection, its four neighbors (the electrodes above, below, left and right) were added to it. If this caused the selection to contain more than the 1024 possible channels, the initial selection was shortened and the process was repeated until the selection contained 1024 non-isolated electrodes. In the rest of the text this selection method is referred to as the deviation-based method.

The quality of the selection was assessed by manually sorting selected electrodes using the UltraMegaSort 2000 program [69, 70, 71], with the intention of verifying qualitatively that the electrodes captured signals that could be clearly separated and classified.

## 2.4 Spike Sorting

In order to identify the number of different cells present in a MEA recording and to assign each action potential to a cell, it is necessary to spike sort the data. The basic and most common approach for spike sorting in MEAs is to i) perform a threshold-based spike detection, ii) extract the spike waveforms i.e. the signals around the spike times, iii) obtain the most relevant features of the waveforms by dimensionality reduction with principal component analysis (PCA) and iv) cluster the waveforms based on their projections along the relevant PCs, assigning each spike to a unit or putative neuron [52, 72, 73]. Although this is an effective method for MEAs with low electrode counts, it cannot be directly applied to HD-MEAs such as the MEA1K.

The high electrode count of the HD-MEAs causes three problems that prevent common spike sorting techniques from working effectively: firstly, if all the electrodes are considered for the spike waveform extraction, the feature space of the waveforms becomes enormous, making the process of feature extraction and classification much harder (a phenomena known as the “curse of dimensionality” [74], common to many domains); secondly, with these devices it is common to record spikes with temporal overlaps; and finally, the vast amount of data makes manual supervision of the sorting process nearly impossible and imposes the need for fully automated methods.

In order to overcome these problems, a new method was proposed by Diggelmann et al. [75, 76]. This new approach, implemented in a program named MySort, subdivides the electrodes in groups based on their spatial location, performs entirely automated sorting on each group and then merges the results removing redundant units. Briefly, the method works through the following steps:

1. -Subdivision into Local Electrode Groups (LEG): First the electrodes are separated in groups of at most 9 electrodes. Each electrode is assigned to at least one LEG, with the aim of grouping together neighboring electrodes

while keeping the total number of groups and the overlaps to a minimum.

2. Spike detection and waveform analysis: The action potentials are detected using a threshold defined on the basis of the standard deviation of the noise on each channel. The precise spike time is defined as the point within a short interval  $\Delta t$  after threshold crossing in which the signal reaches its maximum amplitude. After detection, the waveforms are extracted from all electrodes in the same LEG yielding a vector containing the multi-electrode waveform for each spike.
3. Feature Selection and Clustering: A random subset of spikes is used to define the putative neurons on each LEG. The multi-electrode waveforms of the spikes are first pre-whitened to approach the distributions of each feature to a standard normal distribution, as described in Franke et al. and Pouzat et al. [57, 77]. The waveforms are then subjected to a principal component analysis (PCA) for dimensionality reduction. The projections on the first principal components are used as the defining features of the spikes, which are clustered using mean-shift clustering [78]. Each of the resulting groups or clusters represent the signals emitted by different putative neurons. Those clusters containing less spikes than a given threshold are discarded to prevent outliers from creating a separated group on their own.
4. Template Matching: The averaged multi-electrode waveform on each cluster is used as the template for each putative neuron. All the spikes are compared against the existing templates on the corresponding LEG and assigned to the one which they resemble the most.
5. Cluster merging: Once each spike is assigned to a template, the templates are re-calculated by computing the average waveforms. This is done considering all the assigned spikes, instead of only the ones present in the initial random subset. This process provides more reliable templates, as these are obtained from more samples. The templates are then compared to each other and merged if their similarity is higher than a certain threshold. This is done iteratively, re-computing the templates of any two groups that are merged and comparing the newly obtained templates until no groups can be merged.
6. Duplicate resolution: Cells with large signals that spawn across distant electrodes or whose signal is picked up by electrodes at the intersection of two LEGs can generate duplicates, i.e. putative neurons detected on different LEGs that correspond to a single real neuron. In order to remove these duplicates, the templates obtained from the different LEGs are compared, both in terms of their waveforms and their spike trains (the time series of their spike events). Those templates with high similarity are considered redundant, and in these cases only the template with the largest signal amplitude is kept.

The result of this spike sorting process is a list of detected units or neurons and the assignment of each detected spike to one of the neurons on the list. In the text below, the terms unit and neuron are used interchangeably to refer to the putative neurons detected by the MySort method.

#### 2.4.1 Quality assessment

The quality of the sorting was determined by obtaining statistics on the behavior of each of the detected units. For each unit, the estimated number of missing spikes, the firing rate, the percentage of refractory period violations (RPVs) and the distribution of spike amplitudes were considered.

To obtain the estimated number of missing spikes for each unit, first a normal distribution was centered at the mode of the distribution of amplitudes. Assuming that the normal distribution represents a good estimate of the real distribution of amplitudes, the part of the distribution that fell below the AP detection threshold (5.5 times the standard deviation) represents the spikes that were not detected due to their low amplitude. The same normal distribution was used to estimate the percentage of spikes outside the  $\mu \pm 3\sigma$  range, indicating how well the actual distribution of spike amplitudes fitted to a normal distribution. The percentage of RPVs was calculated as the percentage of inter spike intervals (ISIs) below a 3ms threshold.

A threshold was used for each of these characteristics, so that units with more than 10% estimated missing spikes, more than 5% RPVs, more than 10% of spikes outside the  $\mu \pm 3\sigma$  range or with a firing rate smaller than 0.5 spikes per second were discarded.

### 2.5 Characterization

According to the study by Muller et al. [1], the closed-loop stimulation protocol was expected to alter the connectivity of the neural network. However, a whole set of additional features were computed on each culture so that other possible effects of the stimulation could be observed. These features are divided into four categories: basic features, bursting behavior, connectivity, network properties. The statistical significance of the differences in each of these features was ultimately assessed using a Mann-Whitney U test [79] ( $\alpha = 0.05$ ).

#### 2.5.1 Basic features

On each culture, the firing rate, mean amplitude and amplitude standard deviation were calculated for each of the detected neurons.

#### 2.5.2 Bursting behavior

In order to detect bursting periods, the following method was implemented: the spike trains of all the detected neurons were combined and binned into bins of 50ms. The resulting spike frequencies were smoothed with a Gaussian kernel. The distribution of smoothed spike frequencies was then modeled as a mixture

of two Gaussian distributions, representing tonic firing and bursting regimes. The Gaussian distribution with higher frequencies was used to set thresholds for network burst detection. All time bins with frequencies higher than the mean of the high-frequency Gaussian minus one standard deviation were initially labeled as network bursts. These network bursts were merged whenever the distance between them was shorter than 120ms. After merging, the bursts shorter than 100ms or with less spikes than half the number of detected units, were discarded.

Using the network-bursting periods, the following features described by Cotterill et al. [45] were computed:

- Burst rate: bursts per minute.
- Burst duration: duration of each burst in seconds.
- Within-burst firing rate: mean firing rate within all bursts, in spikes per second.
- Coefficient of variation (CV) of Inter burst intervals (IBI): ratio between the standard deviation and the mean of the lengths of the IBIs.

Additionally, in order to further examine the bursts, the following features were computed:

- IBIs: list of all IBIs in seconds.
- Bursts sizes in number of spikes.
- Bursts sizes in number of neurons involved.

### 2.5.3 Connectivity

The connectivity between the detected neurons was examined using two different surrogate measures:

- Summation over spike trains cross-correlograms defined by P. Dayan and L.F. Abbott [80]
- Spike Time Tiling Coefficient, developed by Cutts and Eglen [55]

Both of these measures were normalized by harmonic averages of the firing rates for each pair of neurons, in order to reduce their dependency with the activity levels of the neurons. The connectivity was assessed using only the spikes observed outside the bursting periods, in order to avoid accounting the participation in network bursts as functional connectivity.

### 2.5.4 Network properties

In order to examine the network properties, the Brain Connectivity Toolbox [81] was used to compute basic centrality measures (in-degree, out-degree) and to measure the modularity of the network.

The usefulness of these measures extends beyond this study and can potentially be applied to any recording done on a MEA platform. Therefore the MATLAB code developed to implement these measures was made available publicly through GitHub [82] at <https://github.com/leo-gg/neurofun>.

## 2.6 Closed-loop Stimulation

The basic principle in the closed-loop stimulation is that an electrical pulse is delivered through one of the channels on the MEA1K chip when a determined event (usually an AP) is detected on another channels. The channels are referred to as stimulation and readout respectively. In this case this was achieved by linking the hardware filter present on the FPGA to the stimulation channel in the MEA1K chip. The C++ interface for the MEA1K was modified to include commands for i) selecting the detection channel (readout), ii) setting the peak detection threshold, iii) activating the closed-loop, iv) setting the refractory period for the detection after the stimulation and v) setting the desired delay between detection and stimulation.

On top of the C++ FPGA interface, a Python script was developed to implement a specific stimulation protocol. The Python script contained commands to specify the channel routing (so that the desired electrode configuration was used), the readout and stimulation channels, the detection parameters for the hardware filter and the stimulation parameters, which described the stimulation pulses shape, width and amplitude. The complete python script used for the closed-loop stimulation is provided in Annex II (6.2).

Initially the AP detection through the hardware filter was done by first estimating the standard deviation of the signal in the readout channel and then using a threshold of 5.5 times the standard deviation value to identify APs. However, the resolution of the hardware filter was found out to be very poor, thus no proper estimation of the channel standard deviation could be one. Instead, it was observed that a clear threshold between noise and high amplitude peaks existed (see figure 4) and thus a value of -200 bits was used as a fixed threshold. The stimulation pulse used was a biphasic quadratic pulse, first negative and then positive, with an amplitude of 61.53mV and a width of 8 samples.

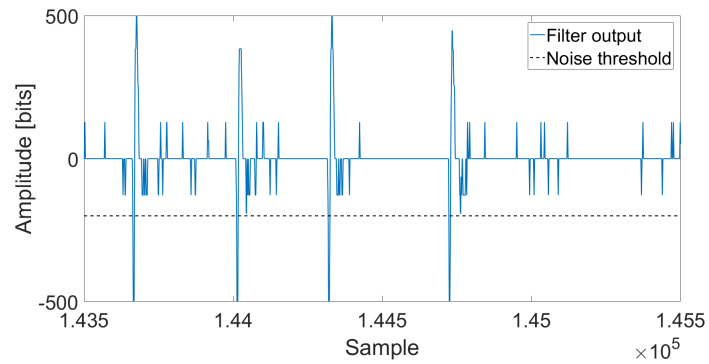


Figure 4: Trace obtained from the hardware filter. The blue line indicates the amplitude of the output signal from the filter. The dashed line in black marks the threshold set for peak detection. The low-resolution filter causes the noise to appear as low amplitude peaks (below -200 bits). Actual APs are seen as very large amplitude deflections.

## 3 Results

### 3.1 Deviation-based electrode selection improves over current methods

The deviation-based method implemented here for the selection of electrodes on the MEA allowed to obtain recordings capturing strong, clean signals. Figures 5, 6 and 7 show the AP waveforms of the best electrodes selected according to different criteria. As it can be seen in Figures 5 and 6, the most active channels and the ones with the largest amplitudes contained noisy non-homogeneous waveforms. On the other hand, as shown in Figure 7, the electrodes ranking highest according to the deviation-based method present uniform waveforms with low noise levels.

The sorting process involved evaluating the footprints of the neurons, for which their waveforms need to be observed in several electrodes. Thus, recording from isolated electrodes impairs the sorting process. In order to avoid this problem, the initial selections were populated with neighboring electrodes. On the first trial (22 DIV), the electrode selection in the control chip contained 1024 electrodes, 723 from the ranking and 301 added neighbors. The selection on the stimulation chip had 1023 electrodes, 687 of which were from the ranking. On the second trial (26 DIV), the selection on the control chip had 1023 electrodes, with 719 coming from the ranking. The selection for the stimulation electrode had 1023 electrodes, 684 coming from the ranked list. This indicates that in all cases there was a significant number of isolated electrodes in the original ranking and in principle could indicate low redundancy, i.e. few good electrodes capturing “good quality” spikes from the same source were included in the ranking.



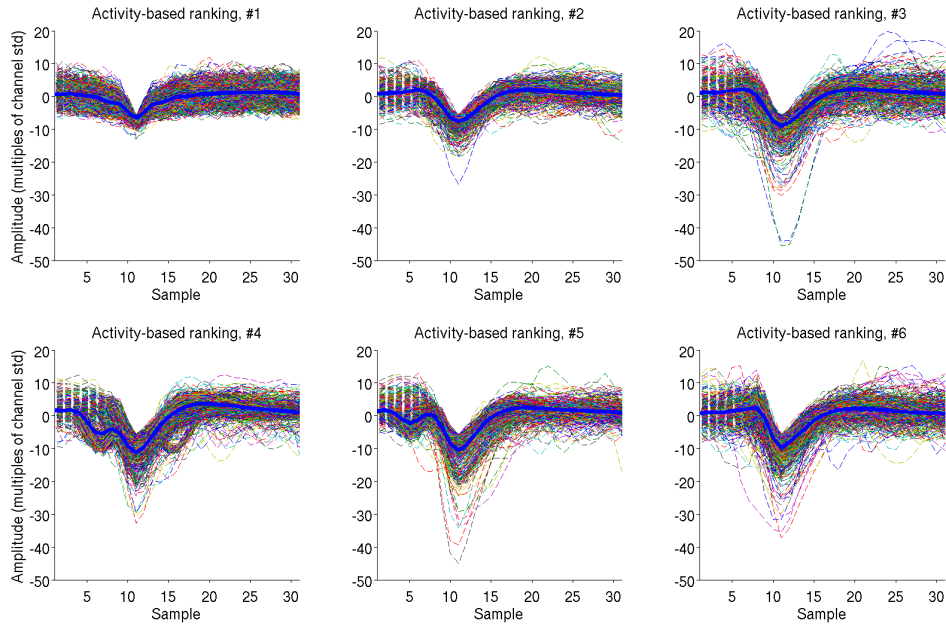


Figure 5: Waveforms of the peaks detected on the six electrodes with the highest activity. Each panel shows the waveforms of all the detected spikes on a given electrode in a different color, with a discontinuous line. The average of all waveforms is shown as a thicker, continuous blue line. The amplitude, given in multiples of the standard deviation of the signal on each channel, clearly indicates that the spikes on these electrodes were small. Also, on the panels for the electrodes ranking #3 to #6, a high number of spikes exhibit a clear deviation from the mean, suggesting an elevated noise level.

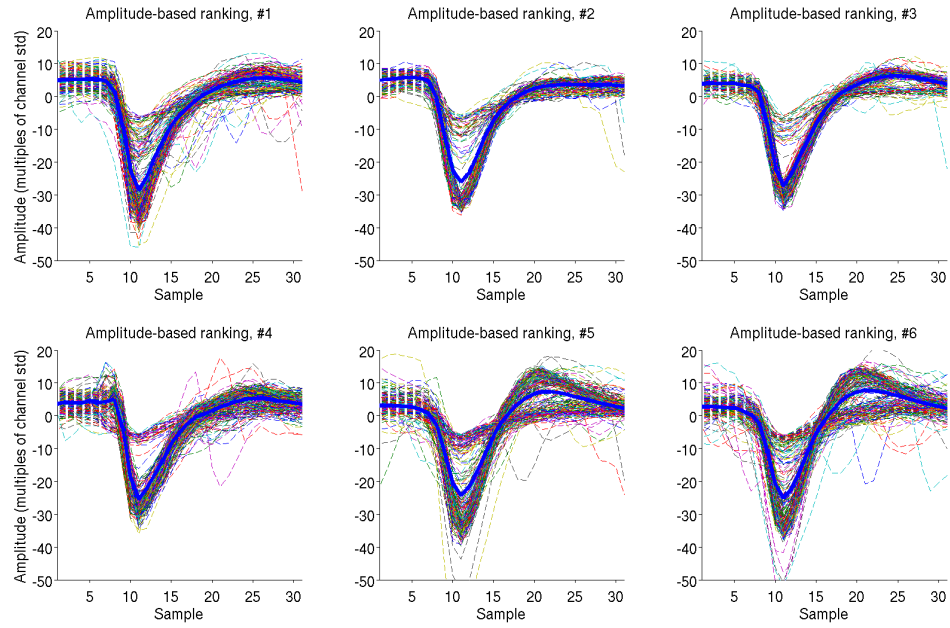


Figure 6: Waveforms of the peaks detected on the six electrodes with the largest amplitudes. Each panel shows the waveforms of all the detected spikes on a given electrode in a different color, with a discontinuous line. The average of all waveforms in shown as a thicker, continuous blue line. In this case the spikes are large on average, however all panels present a large number of spikes with clear deviations from the mean waveform.

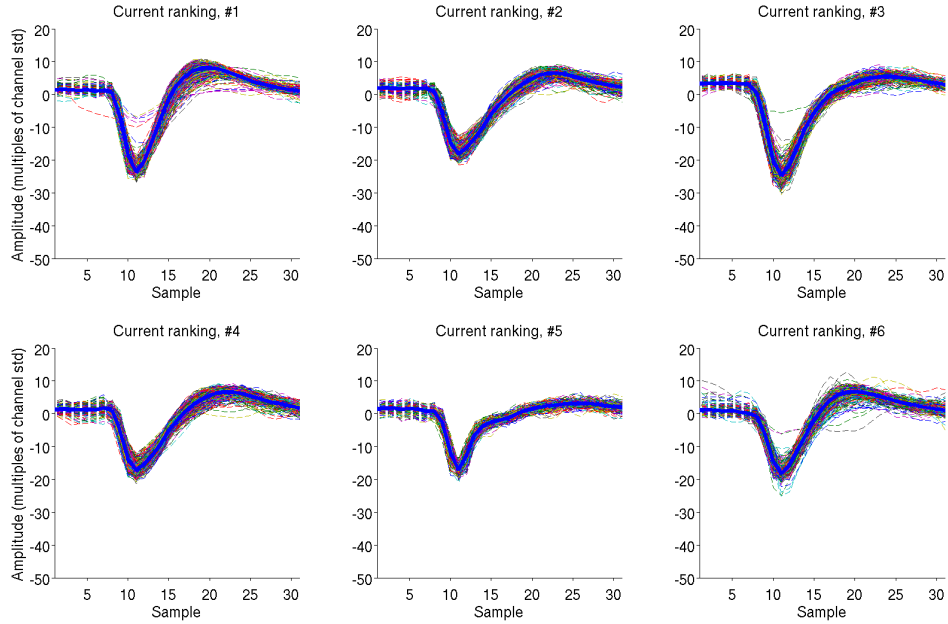


Figure 7: Waveforms corresponding to the six top-ranking electrodes according to the deviation-based method. Each panel shows the waveforms of all the detected spikes on a given electrode in a different color, with a discontinuous line. The average of all waveforms is shown as a thicker, continuous blue line. Only few spikes present large deviations from the mean. In all cases, the mean amplitudes are below ten times the standard deviation of the channel, indicating strong signals.

Manually sorting the electrodes in the selection confirmed that their signals could be easily separated into few different units. Figure 8 illustrates this with an example from electrodes recorded on the control chip after 22 DIV. The filtered signal from the first electrode in the selection ranking plus its 4 closest neighbors is fed to the UltraMegaSort 2000 (UMS2K) program. For each spike detected on any electrode, UMS2K collects a waveform using the 9 samples before the detected peak and the 10 samples following it on all the electrodes. Thus each detected AP has an associated waveform with dimensions  $30 \times 10$  (samples times electrodes). A PCA projection is used to reduce the dimensionality of these waveforms and then k-means clustering is used to separate them into groups. In the case of the first electrode of the ranking, the projection of the waveforms along the two first principal components shows two well differentiated, non-overlapping groups could be clearly identified. This is confirmed by the average Silhouette values of each cluster: 0.766 (cluster 1) and 0.753 (cluster 2). Observing the average waveform of the spikes assigned to each

cluster, it can be seen that the spikes in the first cluster have large amplitudes and a typical AP shape. On the other hand, the average waveform of the spikes assigned to the second group have an amplitude close to zero, suggesting that this group is basically noise.

A similar analysis for the electrodes in the selection that scored lower in the ranking (entries 360 and 723) is shown in Figures 9 and 10. It can be seen that the electrode from the middle of the ranking still presented a high number of actual spikes whereas the last electrode from the ranked list included in the selection contained mostly noise and a few low amplitude spikes. Only 12% of the peaks detected by UMS2K appeared to correspond to actual spikes, and their waveforms had very low amplitude. However, the spikes could still be clearly distinguished from the noise.

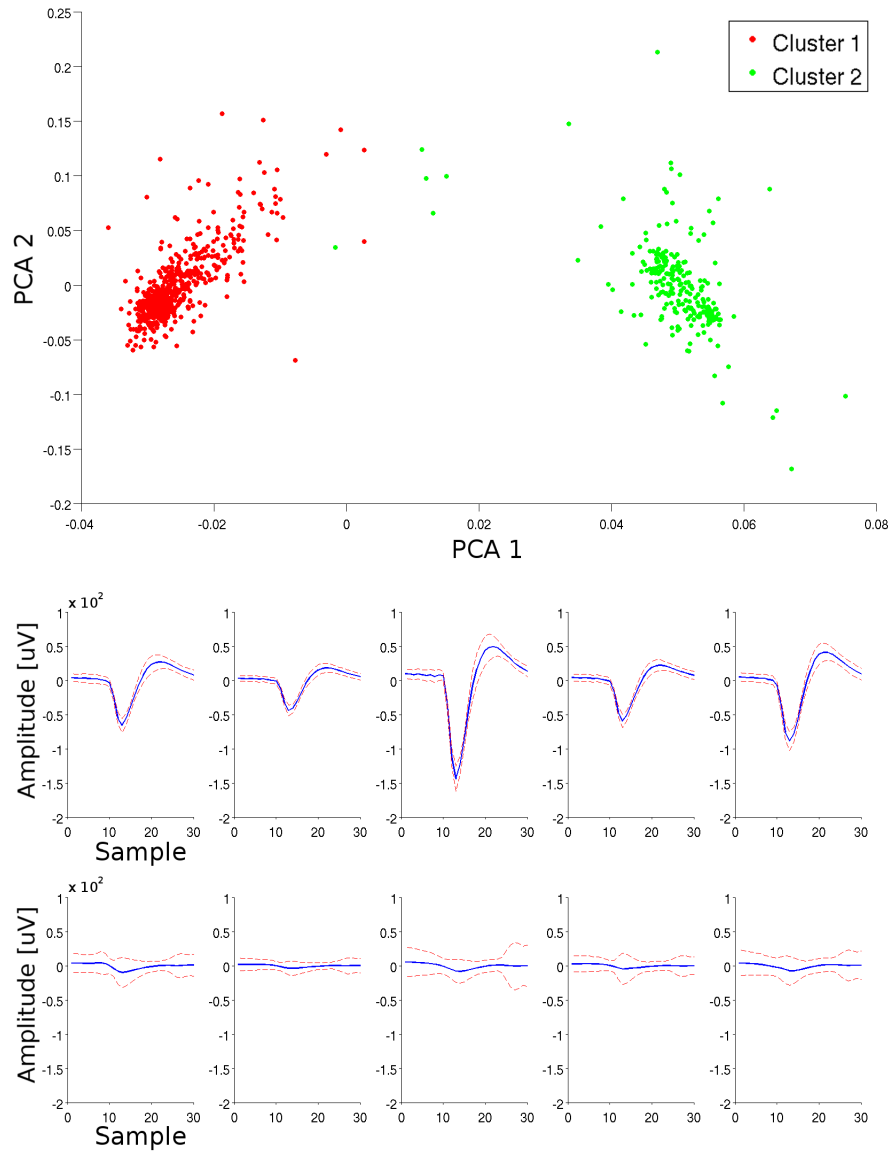


Figure 8: Manual sorting of the top-ranking electrode and its four closest neighbors. The sorting resulted in two clearly differentiated units. The top panel shows the projection of the waveforms on the first two principal components (PCAs). The waveforms assigned to each unit appear in two clearly separated clusters; one was assigned 507 spikes (red) and the second 257 (green). The bottom panel shows the waveforms of each detected unit. Each plot shows the waveform of the spikes on one electrode. The blue line indicates the average waveform and the red dashed line the values two standard deviations above and below the mean. Cluster 1 (top row), exhibits a typical AP waveform whereas cluster 2 (bottom row) displays low amplitude signals, which do not resemble APs and can be discarded as noise. 27

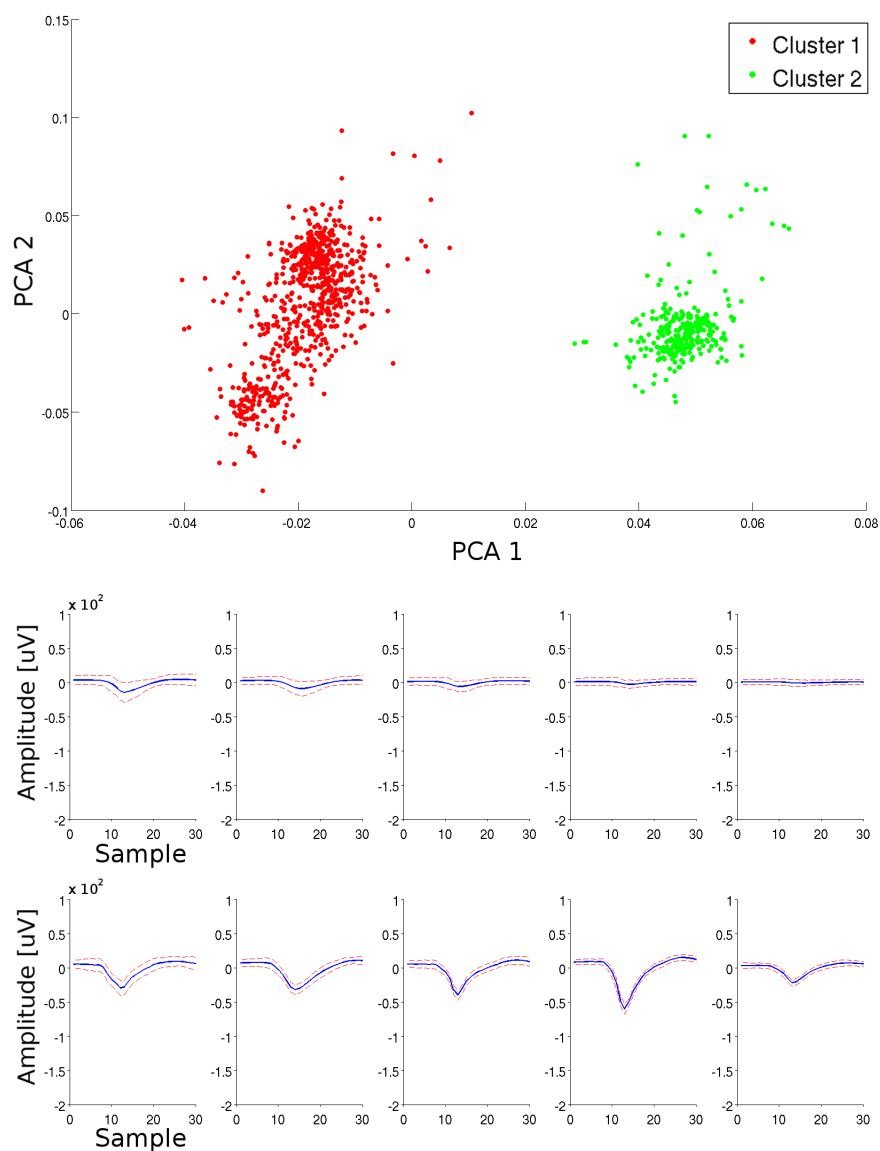


Figure 9: Manual sorting of the electrode from the middle of the ranking and its four closest neighbors. The top panel shows the projection of the waveforms on the first two principal components (PCAs). Again in this case two clear units are clearly distinguished in the PCA projection. The waveforms from both units are shown in the bottom panel. The waveforms on the top row correspond to cluster 1 and those on the bottom row to cluster 2. The blue line indicates the average waveform and the red dashed line the values two standard deviations above and below the mean. A clear distinction can be seen, with cluster 2 exhibiting AP-like shapes and cluster one having very low amplitude signals, which can be seen as noise.

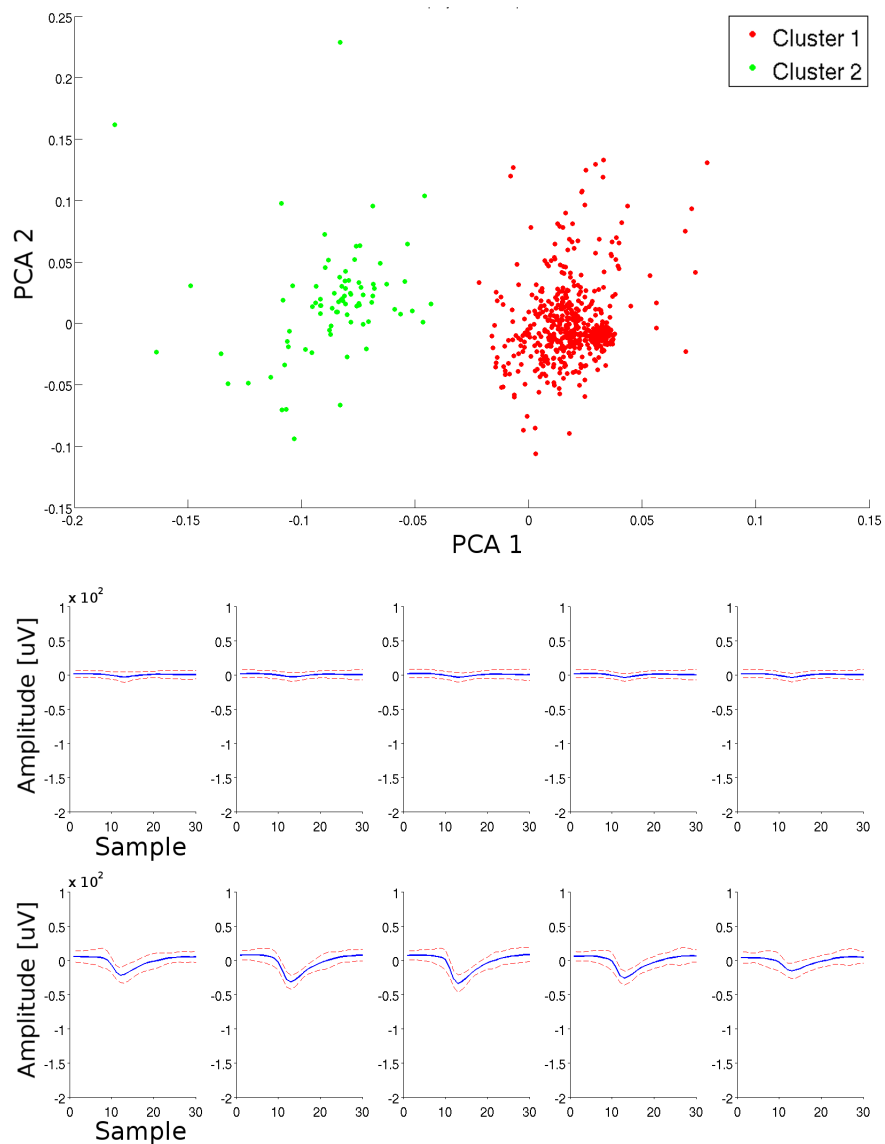


Figure 10: Manual sorting of the electrode from the bottom of the ranking and its four closest neighbors. The top panel shows the projection of the waveforms on the first two principal components (PCAs). Here, the “worst” electrode according to the deviation-based selection method shows separable units. The clusters in PCA space are not as tight as in the examples shown in Figures 8 and 9, but can still be clearly separated. The bottom panel shows the waveforms of each detected unit. Each plot shows the waveform of the spikes on one electrode. The waveforms still show a unit with APs (bottom row) and a unit with very low amplitude signal or noise (top row), although the amplitudes in this case are much lower than in the two other examples.

When applied to the chips, the electrode selection exhibited variability across time. On the control chip, 523 (51%) of the electrodes remained the same, whereas in the chip that was stimulated 399 (38.9%) of the electrodes in the selection were the same on both days as can be seen in Figure 11.

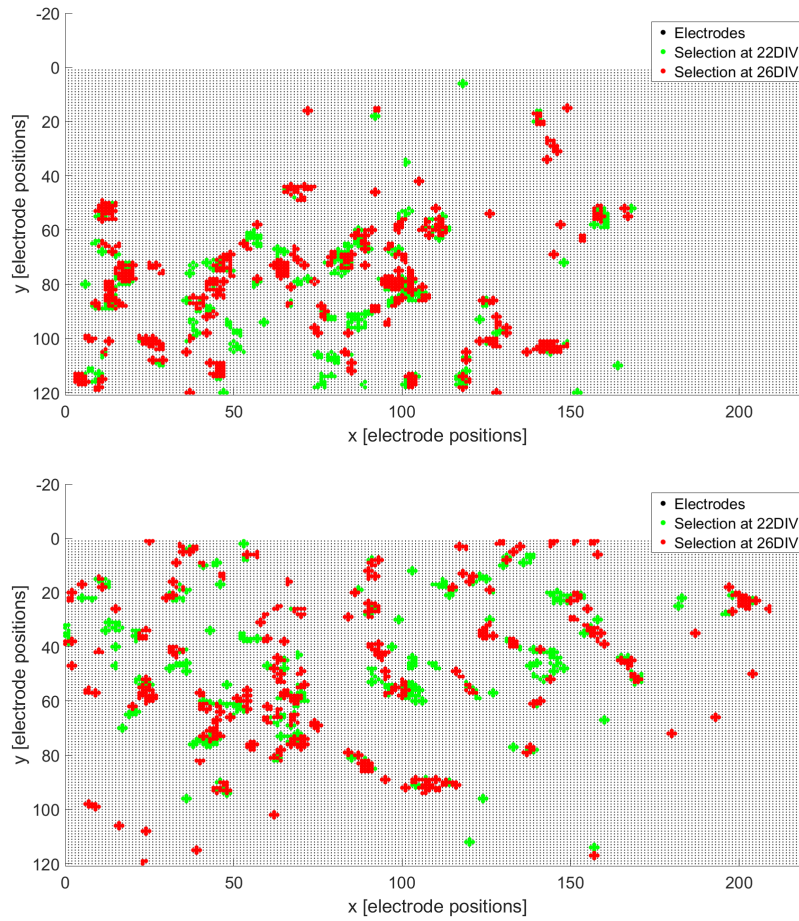


Figure 11: Location of the electrodes selected using the deviation-based method at 22 and 26 DIV. The top panel shows the stimulated chip and the bottom one shows the control. The black dots indicate the electrode locations in the array. The green and black circles indicate the location of the detected units at 22 and 26 DIV respectively. The location of each unit was estimated as the average location of the electrodes in which peaks assigned to the given unit were detected. Both panels show that although the unit appeared in the same areas, the precise location of the detected neurons changed between the two days.



### 3.2 Automated spike sorting obtains poor results from cortical cultures recordings

The sorting was performed automatically using the MySort program. For each chip all the data from each stimulation experiment was combined and sorted together. Table 1 indicates the number of sorted units found on each case and the results of the quality assessment. The results on the table indicate the vast majority of the detected units had very low activity and/or the amplitudes of their peaks followed non-normal distributions. Removing all the units that did not meet the quality requirements resulted in roughly 95% of the units being discarded. Although the remaining units were still numerous and could be used to assess the behavior of the networks, the high number of discarded units indicates a major problem in the sorting process. Given the results of the manual sorting presented in the previous section, it was expected to see a much larger number of detected units complying with the quality criteria. The quality measures implemented here were enough only to detect that there was an issue. A much more extensive analysis would be required to elucidate what specifically is causing the sorter to detect so many units with abnormal amplitude distributions or low firing rates.

Condition	Detected Units	RPVs > 5%	Missing spikes > 10%	Firing rate < 0.5 spikes/s	Spikes outside $\mu \pm 3\sigma$ >10%	Remaining units	
22 DIV	Control	1824	389	165	1202	1027	90
	Stim	2250	283	215	1770	1244	85
26 DIV	Control	1756	333	232	962	1065	123
	Stim	2030	217	228	1480	1194	100

Table 1: Sorting results. The first column indicates the total number of detected units as reported by MySort. The following columns indicate the number of units that did not meet the quality criteria on each case. The last column shows the number of units on each case that fulfilled all the criteria. Each of the features used for the quality assessment is described in methods section (2.4.1).

Like the electrode selection, the number of detected neurons changed between 22 and 26 DIV. Figure 12 shows the location of the detected neurons on both days on the stimulation chip. As it can be seen in the figure, the detected neurons, just like the electrodes, had different locations on each recording.

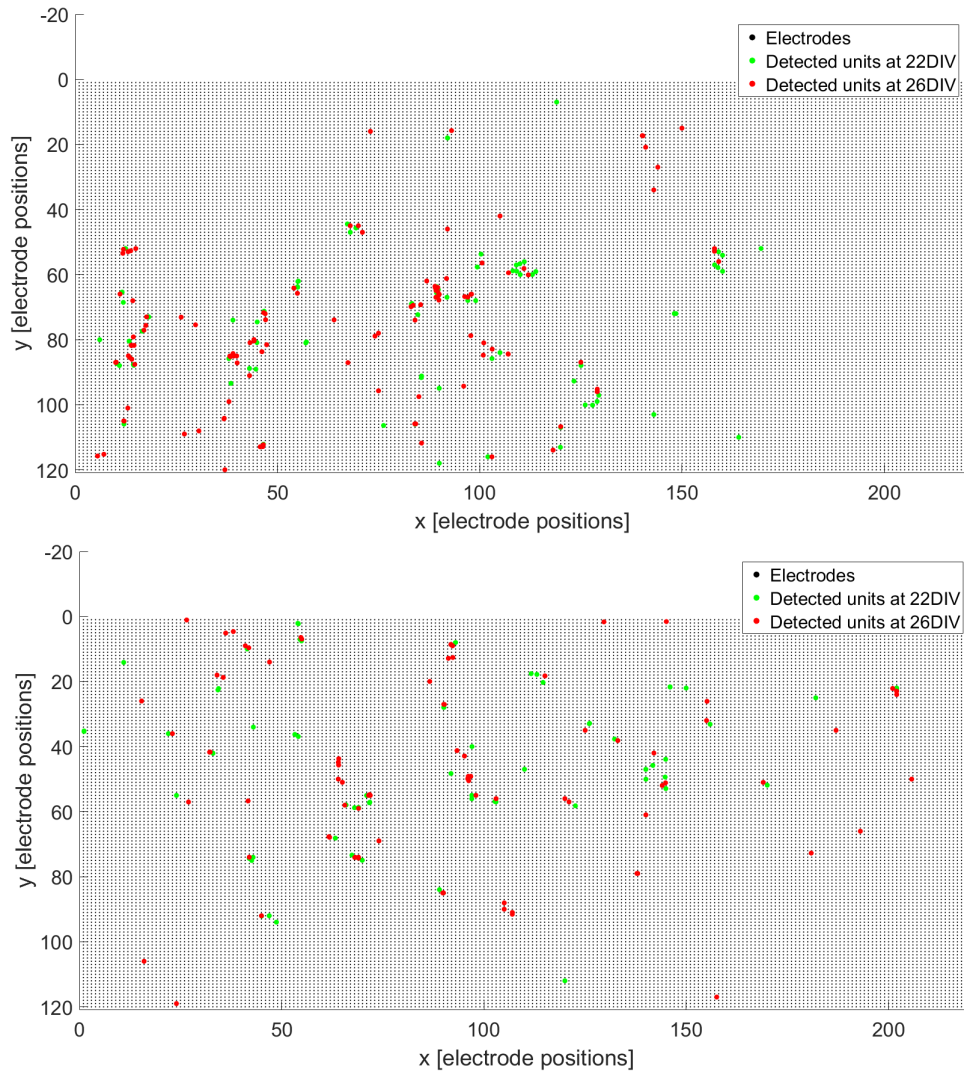


Figure 12: Location of the units detected using MySort after discarding the units that did not meet the quality criteria. The top figure shows the stimulated chip and the bottom figure shows the control.

Several of the units detected on the stimulation chip appeared very close or even overlapping each other. The footprints (the average spike waveforms on all electrodes) of the nearby neurons indicated that these were in fact the same cells with small changes in waveform amplitudes. Two such cases are illustrated in Figure 13. In these instances, one cell was active almost exclusively before the stimulation whereas the nearby or overlapping one became active only after the stimulation. This indicates that the stimulation induced changes in

the waveform amplitudes. In order to compensate for this effect, the detected neurons on the stimulation chip were clustered based on their location and the activities of all the cells in each cluster were added together.

The detected units on the stimulation chip were clustered with a  $17.5 \mu m$  threshold, so that units separated by less than the distance between two electrodes were grouped together. The location of the clustered cells is shown in Figure 14. As indicated in the figure, the number of units was reduced to  $\sim 50\%$  and  $\sim 54\%$  on the first (22 DIV) and second (26 DIV) trials respectively.

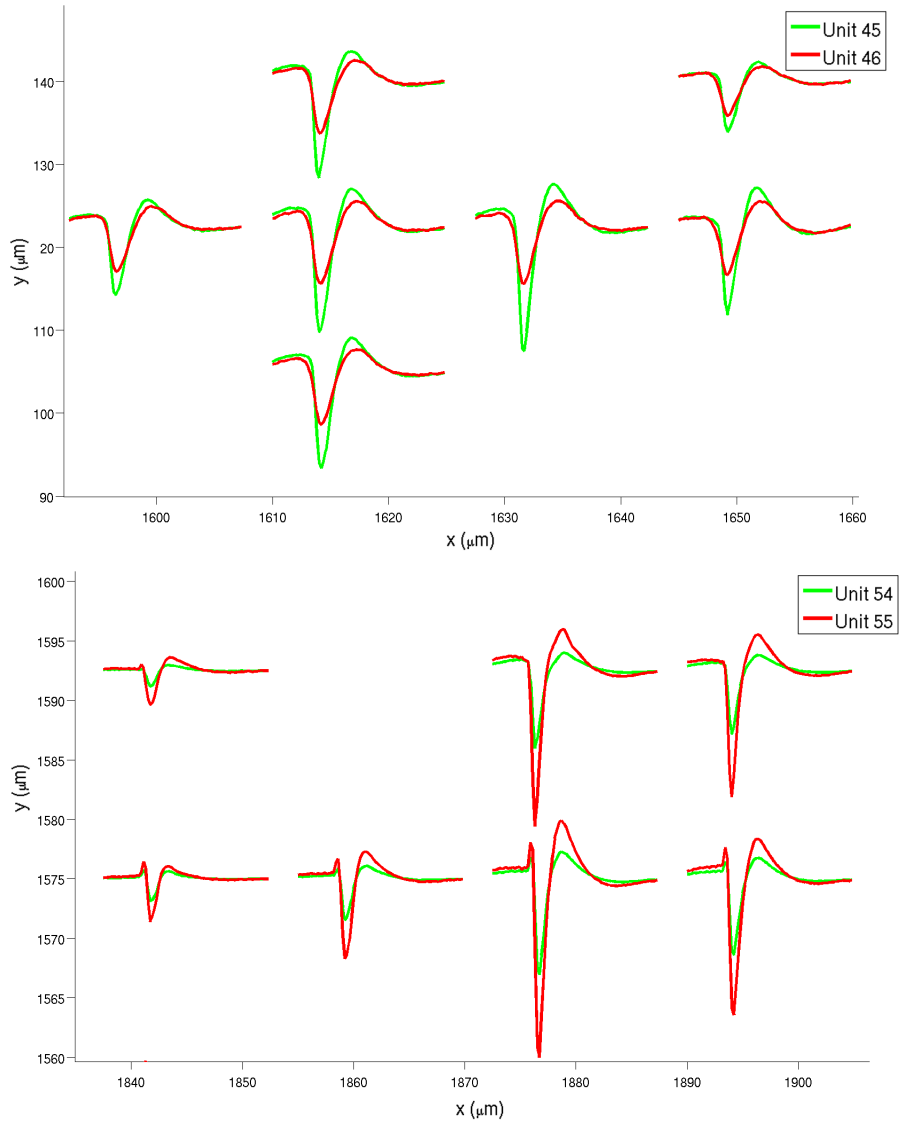


Figure 13: Examples of units with overlapping footprints. A different example, including two different units observed in a given set of electrodes, is shown on each panel. The average spike waveform of each unit on the electrodes that exhibited the largest amplitudes are shown. Each waveform is shown in the location corresponding to the electrode where it was detected and the amplitudes are scaled to avoid overlaps in the representation. In both cases it can be appreciated that the overlapping units have similar footprints, only distinguished by changes in amplitude and small changes in their waveforms.

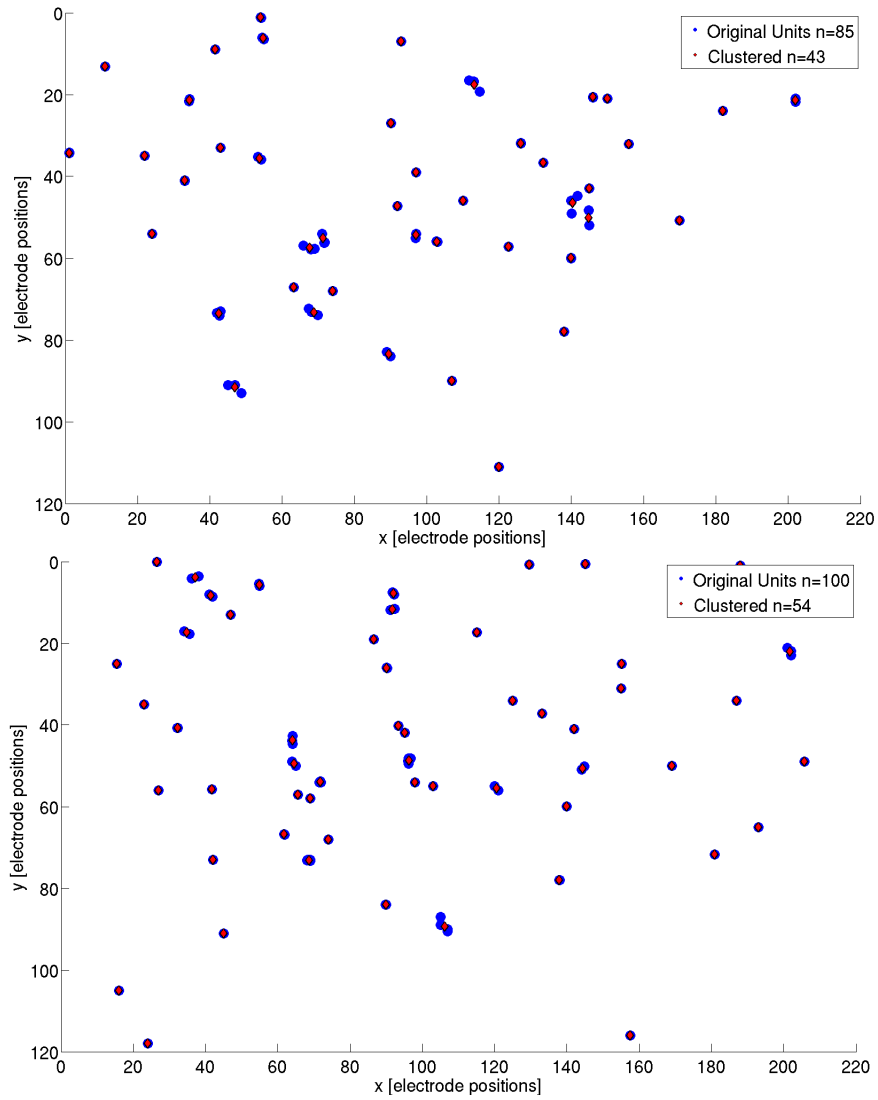


Figure 14: Location of the original detected units and the clustered ones on the stimulated chip at 22 (top) and 26 (bottom) DIV. The blue dots indicate the position of the original units detected in the spike sorting, and the red diamonds show the locations after the nearby units where clustered. The coordinates are given in electrode positions; the electrodes on the chip are arranged in a rectangular grid, with each electrode separated by  $17.5\mu m$  in the horizontal and vertical axes from its neighbors.

### 3.3 Implementation of Closed-loop Stimulation

Figure 15 shows an example trace of the readout and the stimulation channels. As the figure illustrates, a stimulation pulse can be seen every time an AP appears in the readout channel.

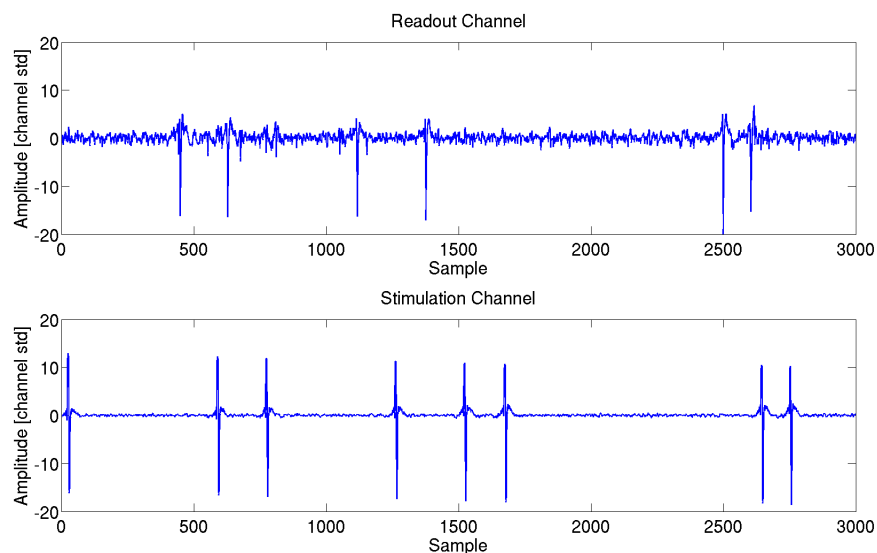


Figure 15: Example traces recorded from the readout and stimulation channels while the closed-loop protocol was being applied. The top panel shows the recording obtained from the readout channel, where six evident spikes appear in the time-frame shown. The panel below presents the signal recorded from the stimulation channel on the same time-frame. A total of eight stimulation pulses can be clearly distinguished in this recording. There is a stimulation pulse following each spike from the readout channels (with the stipulated delay) and additionally two spikes without a preceding AP on the readout channel.

Since the AP detection was carried out using the low resolution hardware filter, there were occurrences of low amplitude negative peaks that were detected as APs and triggered a stimulation pulse. In a one-minute recording, 94.02% of the stimulation pulses corresponded to a preceding AP that could be classified as such by the offline detection method (threshold-based). This implies that there was a 5.98% of false positives or “spontaneous” stimulation pulses. All the detected APs had a corresponding stimulation pulse, thus all the peaks detected as APs offline were also detected by the hardware filter, with no false negatives.

### 3.4 Effects of Closed-loop Stimulation

Each of the chips was analyzed using each of the characteristics described in the methods section. The analysis was performed separately for each of the

recordings: baseline, blank, stimulation and it is divided in three sections: basic features, bursting behavior and connectivity.

### 3.4.1 Closed-loop stimulation causes loss of activity and reduction of AP amplitudes

Tables 2 and 3 show the basic features from each of the cultures obtained from recording. As the values indicate, the units detected on the control chip have similar firing rates, amplitudes and amplitude deviations in the three recordings done after 22 DIV. On the recordings done after 26 DIV, the control chip exhibits lower firing rates and amplitudes and increased amplitude deviations. The units detected on the stimulated chip present homogeneous values in the baseline and blank recordings. Comparing the pre-stimulation recordings from the stimulated chip at 22 and 26 DIV shows that the firing rate remained at the same level, the peak amplitude decreased and the amplitude deviation increased. The values obtained after the stimulation indicate a clear decay in all three features when compared with the pre-stimulation recordings. All these similarities and differences were found to be statistically significant when subjected to a Mann-Whitney U test [79].

Condition		Mean Firing rate (spikes/s)	Mean Amplitude (STD)	Mean Amplitude Deviation
Control	Base	1.3922	25.3357	0.1916
	Blank	1.598	24.8921	0.18
	Stim	1.6042	24.6012	0.1868
Stim	Base	1.24	23.493	0.171
	Blank	1.21	23.511	0.163
	Stim	1.05	17.96	0.091

Table 2: Basic features from both chips obtained from the recordings at 22 DIV. The columns show the mean frequency of spikes from each unit, the mean amplitude of the spikes and the mean standard deviation of the spike amplitudes.

Condition		Mean Firing rate (spikes/s)	Mean Amplitude (STD)	Mean Amplitude Deviation
Control	Base	1.2024	23.1556	0.2345
	Blank	1.2359	22.7846	0.2268
	Stim	1.3235	22.2995	0.2249
Stim	Base	1.2	20.642	0.204
	Blank	1.2238	20.5392	0.1962
	Stim	0.8169	15.914	0.1126

Table 3: Basic features from both chips obtained from the recordings at 26 DIV. The columns show values for the same variables as Table 2.

### 3.4.2 Bursting patterns

Figure 16 shows a comparison of the firing frequencies of each chip on the blank recordings at 22 DIV. This comparison illustrates the qualitative differences observed on the bursting behavior on each case. The control chip exhibits a higher level of tonic firing and its bursts are in general shorter. The stimulated chip on the other hand has much lower levels of tonic firing, which diminishes the threshold for burst detection and causes the bursts to be longer and to contain a higher number of spikes. A detailed quantitative analysis of the bursting behaviors and the effects of the stimulation on them is presented below.

The values related to the distribution of bursts on each of the recordings is shown in tables 4 and 5. According to these values, the bursting rate increases on the control chip from 22 to 26 DIV, with the IBI decreasing accordingly. The values from each day were found to have no statistically significant differences, whereas the increase in bursting rate and decrease in IBI seen from 22 to 26 DIV were both found to be statistically significant. In comparison, the stimulated chip shows lower bursting rates and larger IBIs. Comparing the baseline and blank recordings on the stimulated chip at 22 DIV shows a large, significant spontaneous drift is seen in both the bursting rate and the IBI. A similar change is observed at 26 DIV between the blank and the post-stimulation recordings. Thus no change in the bursting rate or the IBI can be attributed to the stimulation. The values on the stimulated chip show significant differences between the recordings at 22 and 26 DIV only when the blank recordings are compared; considering the magnitude of the spontaneous drift. Thus it can be stated that as opposite to the control chip, the culture on the stimulated chip did not show an increase in the frequency of bursts between 22 and 26 DIV. Finally, the coefficient of variation (CV) of the IBI shows high values in all cases, indicating that the IBI had a large variability in all the recordings on both chips. This means that the spacing between bursts was highly irregular in both cultures.



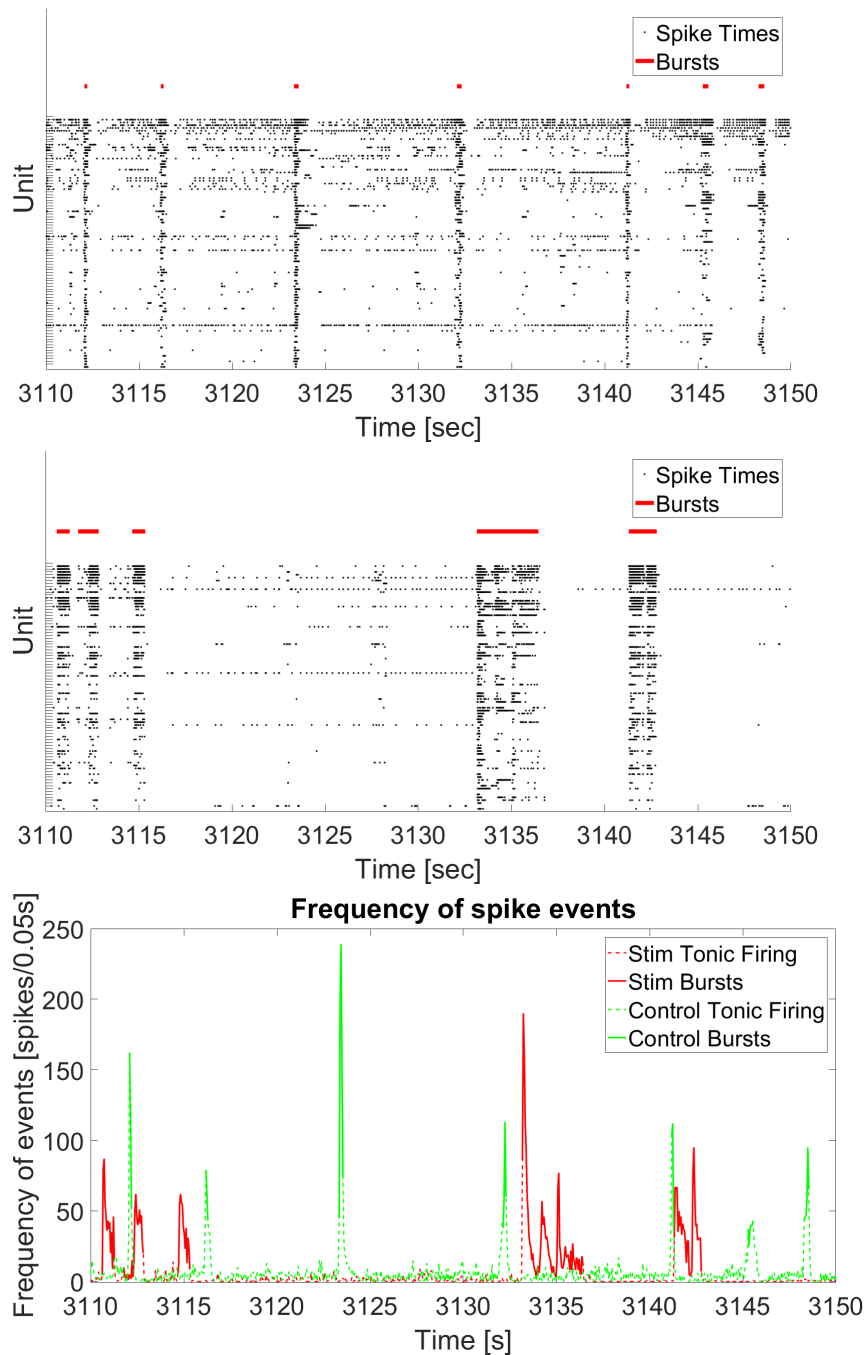


Figure 16: Raster plots and firing frequencies of both chips during the blank recordings. The top panel shows the raster plot of the control chip. A high level of tonic firing is observed, although clear culture-wide bursts are clearly distinguishable. The middle panel shows the raster plot corresponding to the stimulated chip. The stimulated chip has fewer units exhibiting tonic firing and the network-wide bursts have a longer duration. The bottom plot shows the frequency of spikes on both chips. Due to the higher level of tonic firing, the threshold for burst detection on the control chip (green) is higher, reducing the burst duration even further in this case.

Condition		Mean Bursting Rate (Bursts/minute)	Mean IBI (seconds)	CV IBI
Control	Base	7.9807	5.1328	0.7565
	Blank	6.7806	5.9554	0.7456
	Stim	7.5977	5.5147	0.6112
Stim	Base	6.1655	5.4804	0.835
	Blank	4.1352	7.2499	0.7764
	Stim	4.2559	6.7924	0.7976

Table 4: Bursting rates and inter burst intervals (IBIs) and the coefficient of variation (CV) of the IBIs computed from the recordings at 22 DIV. The bursts were detected using the Gaussian-mixture model approach described in section 2.5.2, thus features refer to the ensemble of detected neurons.

Condition		Mean Bursting Rate (Bursts/minute)	Mean IBI (seconds)	CV IBI
Control	Base	10.2467	4.1023	0.8645
	Blank	13.2456	2.98	0.6713
	Stim	12.2945	3.274	0.6328
Stim	Base	6.2936	6.9891	0.8551
	Blank	6.7085	6.5584	0.8049
	Stim	4.7960	5.3691	0.8402

Table 5: Bursting rates and inter burst intervals computed from the recordings at 26 DIV. The columns show values for the same variables as Table 4.

### 3.4.3 Bursts features

The burst size (in number of units and spikes) and duration, together with the firing rates observed within the bursts were calculated for each burst on each recording. The average values for these features are shown in tables 6 and 7. The recordings from the control chip at 22DIV revealed a significant increase in burst sizes (both in number of spikes and number of units involved) and within-burst firing rates on the third recording. Since the control chip was not stimulated, these changes can be considered a spontaneous drift. On the recordings done at 26 DIV there was a significant decrease in the number of spikes per burst, which again can be considered a spontaneous drift. Comparing the recordings from the control chip at 22 and 26 DIV, the number of units per burst increased significantly and the burst duration exhibited a significant decrease in all three recordings. The differences in the within-burst firing rates across days were smaller than across the recordings at 22 DIV. In sum, at 26 DIV the control chip showed shorter bursts involving more units than at 22 DIV.

The stimulated chip shows a rather different behavior: its bursts are much

longer in time, causing them to have bigger sizes in terms of number of spikes even though the firing rates are lower than in the control chip. At 22 DIV, the stimulated chip shows a large spontaneous drift in the burst lengths (baseline and blank recordings) and firing rates. As a consequence, a large difference is also observed in the burst sizes in terms of number of spikes. The post-stimulation recording shows significantly lower firing rates (in accordance with the reduced firing rates shown in Table 2) and a lower number of units involved on each burst, which in turn result in a much lower number of spikes per burst. The recordings at 26 DIV show a similar situation: the post-stimulation recording has significantly lower firing rates and the number of units participating in the bursts is also reduced, causing the bursts to be much smaller in terms of number of spikes. Comparing the recordings of the stimulated chip on both days, the bursts are overall shorter but the differences fall within the range of the spontaneous drift. The number of units involved per burst is significantly larger on the pre-stimulation recordings at 26 DIV as compared to the same recordings at 22 DIV, however there was no significant difference after the stimulation. The firing rates in the pre-stimulation recordings did not exhibit significant differences larger than the spontaneous drifts, and the same happened on the post-stimulation recordings. The number of spikes per burst is clearly smaller after the stimulation on the recordings from 26 DIV, but this can be directly explained by the shorter length of the bursts. To summarize, the stimulation caused a clear decrease of the number of units per bursts and of the within-burst firing rates. This agrees with the observation that the stimulation decreased the firing rates. The only feature that is distinctively changed from 22 to 26 DIV is the burst size in number of units. Yet it is apparent that the sampling here is not sufficient to properly estimate the magnitude of the spontaneous changes.

Condition		Mean Burst Size (Spikes)	Mean Burst Size (Units)	Mean Burst Duration (Seconds)	Mean Within-Burst Firing Rate (spikes/s)
Control	Base	343.9345	64.128	0.0779	63.8573
	Blank	347.2367	65.2332	0.0784	65.9983
	Stim	367.0879	69.8619	0.073	70.3566
Stim	Base	639.8601	52.3823	0.2915	41.28
	Blank	859.4605	60.9671	0.324	45.712
	Stim	433.544	36.8296	0.3851	31.5637

Table 6: Burst properties calculated from the recordings at 22 DIV. The bursts were detected using the combined firing patterns from all neurons, as described in 2.5.2. The columns show the mean sizes of the detected bursts, expressed in number of spikes, number of neurons involved and number of seconds. The last column shows the average firing rate of all neurons during the bursting periods.

Condition		Mean Burst Size (Spikes)	Mean Burst Size (Units)	Mean Burst Duration (Seconds)	Mean Within-Burst Firing Rate (spikes/s)
Control	Base	355.0499	89.8076	0.0539	70.8874
	Blank	369.2395	92.4118	0.0613	68.1771
	Stim	338.9566	86.4872	0.0547	70.9868
Stim	Base	926.7875	77.8750	0.3138	48.9677
	Blank	672.6615	69.7588	0.2514	45.1168
	Stim	229.1398	38.9749	0.2124	28.1809

Table 7: Burst properties calculated from the recordings at at 26 DIV. The columns show values for the same variables as Table6.

#### 3.4.4 Closed-loop stimulation causes loss of connectivity

The connectivity between the detected neurons was assessed using the cross-correlogram method and the STTC. As Figure 17 illustrates, at 22DIV the connectivity in the control chip remained practically unaltered, whereas on the stimulated chip, a clear decrease was observed after the stimulation. The statistical test determined that there were no significant differences among the connectivity distributions on the control chip and that the apparent decrease in connectivity in the stimulated chip after the stimulation was statistically significant for both of the measures used.

The results obtained from the experiment performed at 26 DIV are shown in in Figure 18. The results on this second experiment confirmed the initial

observations: also at 26 DIV the stimulation caused a significant decrease in connectivity while the values obtained for the different recordings from the control chip had no significant differences.

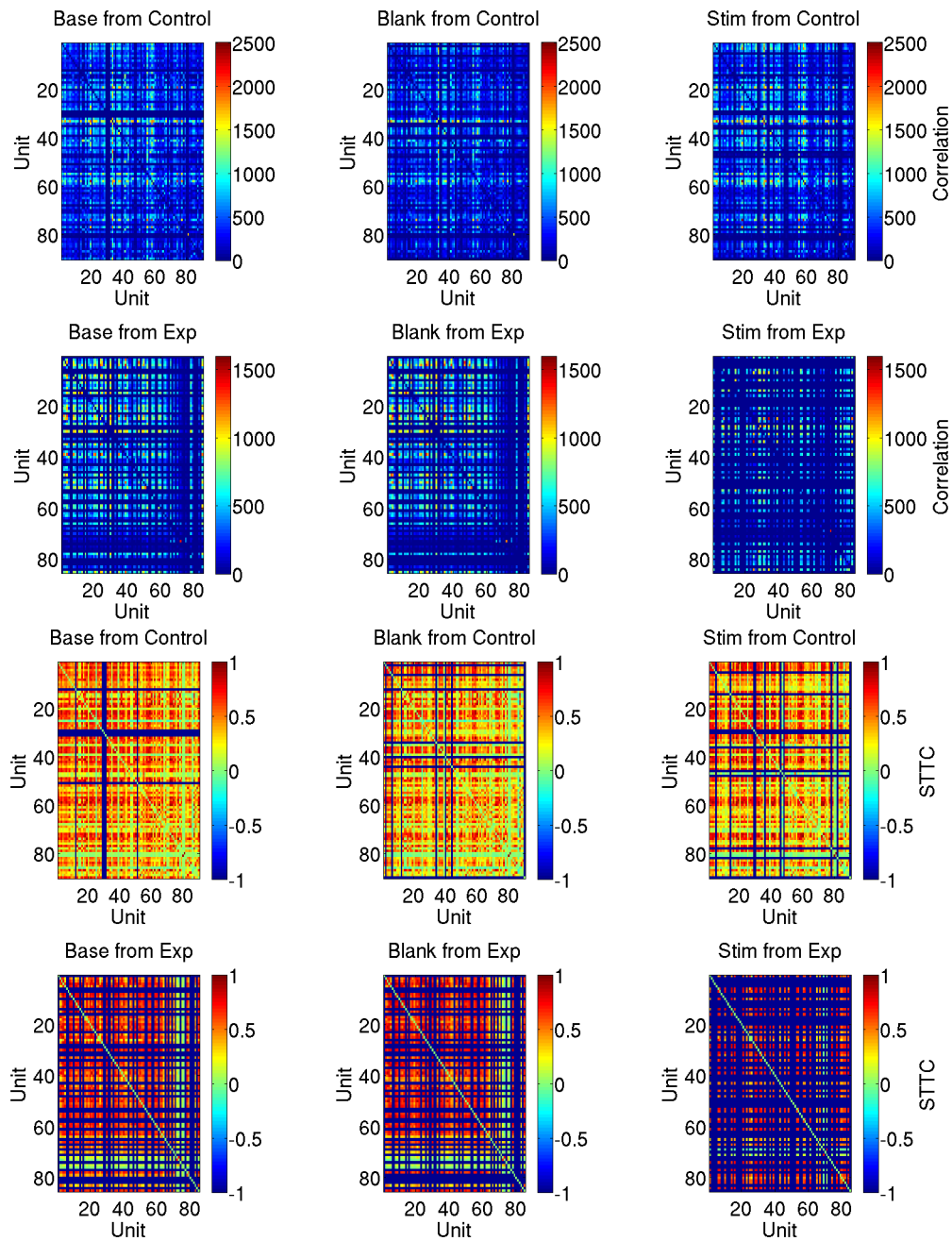


Figure 17: Correlation measurements on both chips at 22 DIV. The first two rows show the cross-correlogram matrices, with the control chip on the top row and the stimulated chip on the second row. The colors indicate the correlation values obtained for each pair of units. The elements in the diagonal have a value of zero, since spikes happening within 1ms of each other are not considered for the summation over the cross-correlogram. The last two rows show the STTC matrices, with the colors indicating the STTC observed for each pair of units.

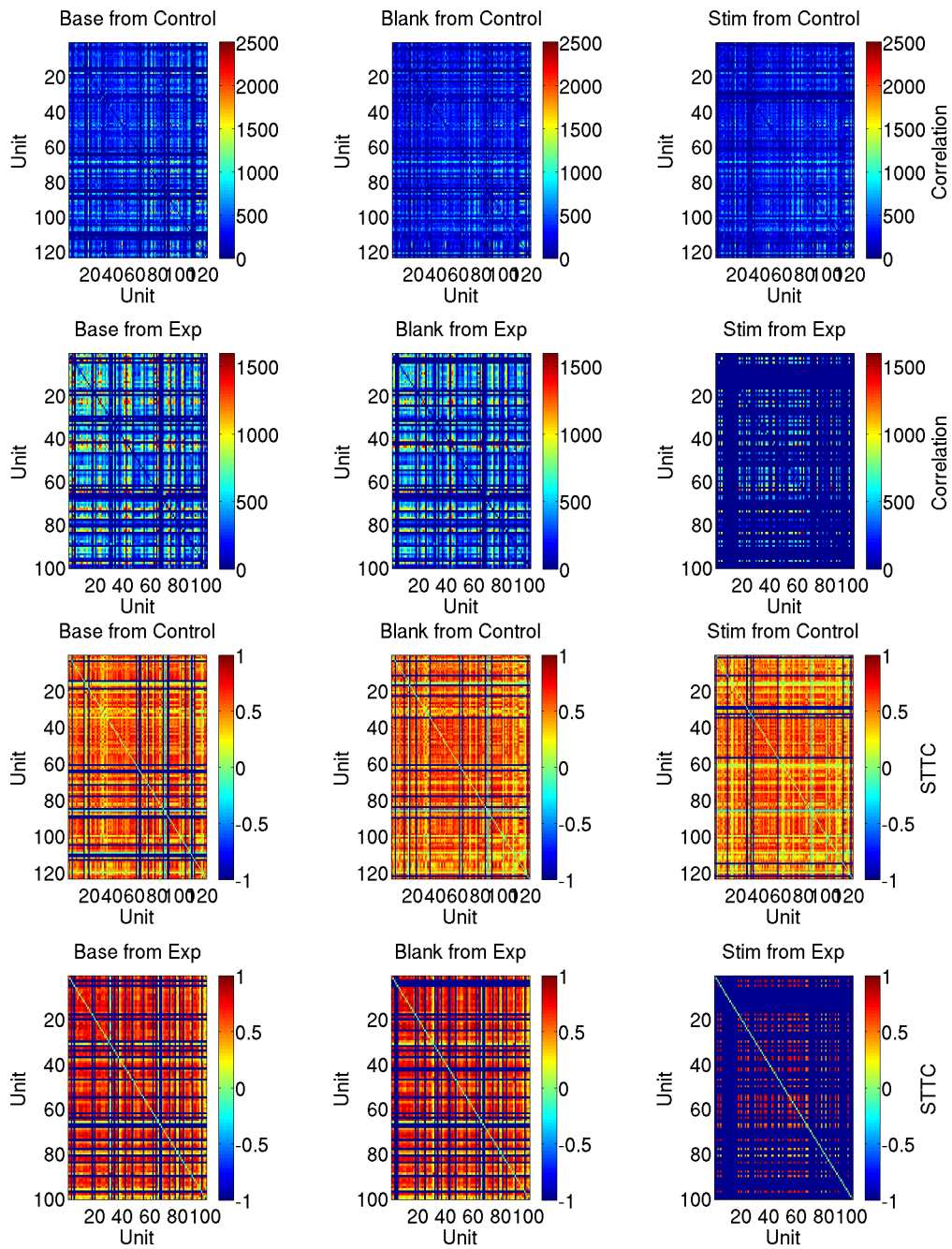


Figure 18: Correlation measurements on both chips at 22 DIV. The correlation values obtained from the cross-correlograms are displayed on the first two rows, with the control chip on top and the stimulated chip on the bottom. The STTC matrices are displayed on the last top rows, with the control chip on the top row and the stimulated chip on the last row.

## 4 Discussion

The method devised to obtain the electrode selection appears to have provided the desired results. Based on the waveform shapes and the PCA projections from the electrodes at the top (Figure 8), middle (Figure 9) and bottom (Figure 10) of the ranking, even without a fully systematic analysis of all the selected electrodes, it can be stated that the method did in fact provide a selection of electrodes with clean signals that could easily be separated into different units (or in which the signals from units could be clearly distinguished from the noise).

The automatic spike sorting resulted initially in a very large number of detected units. Applying few quality control measures reduced this number dramatically, as they indicated that  $\sim 95\%$  of the units should be discarded. The remaining units could safely be considered good quality results and used for further analysis. However it is clear that this process discarded a large part of the data, therefore only a fraction of the neurons in the culture could be taken into account for the functional analysis of the neural network. This result is a clear indication that the spike sorting method was not adequate for the analysis of this type of recording. The MySort program [75] has been successfully used for the analysis of retina recordings, yet it is clear that it needs to be modified before it can be applied to cortical recordings.

The closed-loop protocol was successfully implemented, although the limitations imposed by the hardware filter resulted in a small percentage of stimulation pulses triggered in response to noise rather than actual spike events. Improvements in the hardware filter design could possibly reduce or eliminate this artifact.

Both the amplitudes (Figure 13) and the firing rates (Tables 2 and 3) of the detected units were significantly reduced as a consequence of the stimulation. The changes were not limited in any way to the units located near the stimulation electrode, and were instead seen as a global change in the culture. This effect should be investigated further: it is necessary to discard possible hardware malfunctions and to examine in detail how many APs were triggered with each stimulation pulse. The information available from the present study can however already discard a major artifact or cell death, as the spike frequencies and amplitudes at the electrode level, i.e. the pre-sorted data, do not show significant changes caused by the stimulation (Figure 19). Although there is no explicit analysis of firing rates, the study by Wagenaar et al. [13] shows array-wide decreases of firing rates when cultures are stimulated with frequencies above 1Hz, which is consistent with the results observed here. Moreover, in the subsequent study by Madhavan et al. [83], the “quieting” effect of multi-site stimulation is seen to last for up to 8 hours after the stimulation protocol, an observation consistent with the reversible nature of the stimulation effects seen in the present study.



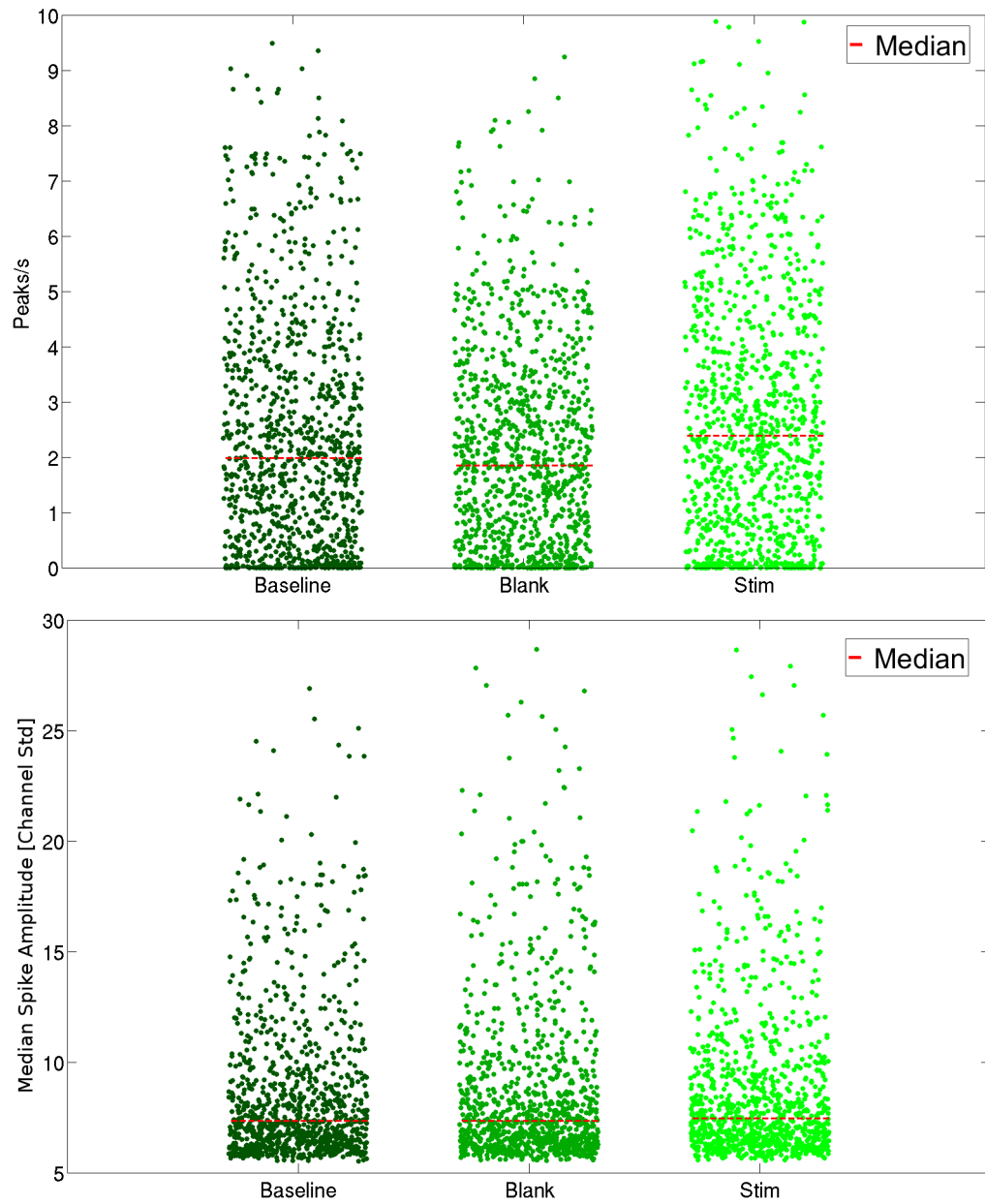


Figure 19: Distributions of spike frequencies and amplitudes at the electrode level, computed from the recordings of the stimulated chip at 22 DIV. The top panel shows the firing frequency per electrode, expressed in detected peaks per second. The bottom panel shows the median amplitudes of the peaks detected on each electrode. In both cases, the median values of the distributions are indicated with a red line.

In accordance with the decreased firing rates, the stimulation causes the stimulated chip to present bursts in which a smaller number of units are implicated and in which these units exhibit lower firing rates. Notably, the bursting rates and IBIs do not seem affected by the stimulation so the temporal structure of the bursting patterns seems to remain unaltered. It is also remarkable to see that unlike the control chip, the level of bursting did not increase in the stimulated chip at 26 DIV. This could indicate that the stimulation had tampered with the developmental process of the network, as it was expected (and observed in the control) for the network to produce more bursts as it develops. The features of bursts also appear to remain more constant in the stimulated chip whereas a clear drift towards narrower, more intense bursts was seen on the control; however the large variation seen in the pre-stimulation recordings points toward a lack of proper sampling of these features. More samples would be required to properly establish the effect of the stimulation on the detailed features of the bursts.

The connectivity, as assessed by the cross-correlogram method and the STTC, presents a clear evidence of the widespread effects of the stimulation. The same effect is seen when either method is used to measure the connectivity between the units, and the results are similar both at 22 and 26 DIV. The decrease in connectivity could in principle be attributed to the generalized loss of activity seen after the stimulation, even though both of the methods used do include a normalization based on the spike rates, which in principle makes both connectivity measures independent of the activity levels.

In summary, these observations seem to indicate that the electrical stimulation caused a widespread inhibition of spiking activity, including a notable decrease in the bursting levels and ultimately being reflected as a network-wide loss of connectivity. In addition, the results suggest that the stimulation on the chip interferes with the normal development of bursting patterns and possibly bursts features. However, given the limited sampling and the methodological shortcomings, these results would still need to be confirmed by further experiments.

## 5 Conclusion

This study presents a successful implementation of a closed-loop stimulation protocol for neuronal cultures based on the MEA1K chip. The study of the effects of the stimulation revealed that the methodologies for the analysis of cultured neuronal networks on high-resolution MEAs are not fully developed. In particular, the spike sorting technique was found not to be adequate and the stimulation effects and parameters clearly need a much more detailed study. In addition, the differences between the two cultures observed before any stimulation had taken place revealed that there is a high degree of variability across cultures, thus a larger number of cultures should be examined in order to determine the normal ranges of values for the different features.

Despite these shortcomings, the present work shows clear and consistent evidence of a reversible, generalized decrease in the firing rate of the detected neurons induced by the stimulation. On the methodological side, this study presents developments in the analysis of data obtained from extra-cellular recordings. Specifically, new approaches for the selection of recording electrodes on the MEA1K and for burst detection are introduced, together with a compilation of methods for the characterization of neuronal cultures, implemented and adapted to be used with data obtained from MEA1K recordings.

In order to improve over the experimental results obtained here, it would be necessary to i) investigate the causes of the low quality of the units detected by the spike sorter and adapt it as needed for its use with cortical neurons, ii) thoroughly investigate the effects of different stimulation parameters on each stimulated neuron, obtaining spike-triggered averages, locating the most suitable stimulation point and then building excitability profiles and iii) sampling a larger number of cultures to observe the distribution of values of each of the features used for the analysis of the networks.

## References

- [1] Jan Müller, Douglas J. Bakkum, and Andreas Hierlemann. Sub-millisecond closed-loop feedback stimulation between arbitrary sets of individual neurons. *Frontiers in Neural Circuits*, 6, 2013.
- [2] D. A. Prince. Neurophysiology of epilepsy. *Annual Review of Neuroscience*, 1(1):395–415, 1978.
- [3] Antonio M. Persico and Thomas Bourgeron. Searching for ways out of the autism maze: genetic, epigenetic and environmental clues. *Trends in Neurosciences*, 29(7):349–358, 2006.
- [4] Huda Y. Zoghbi. Postnatal neurodevelopmental disorders: Meeting at the synapse? *Science*, 302(5646):826–830, 2003.
- [5] Hsiao-Tuan Chao, Huda Y. Zoghbi, and Christian Rosenmund. MeCP2 controls excitatory synaptic strength by regulating glutamatergic synapse number. *Neuron*, 56(1):58–65, 2007.
- [6] Jesse E. Hanson and Daniel V. Madison. Presynaptic *fmr1* genotype influences the degree of synaptic connectivity in a mosaic mouse model of fragile x syndrome. *Journal of Neuroscience*, 27(15):4014–4018, 2007.
- [7] Vardhan S. Dani, Qiang Chang, Arianna Maffei, Gina G. Turrigiano, Rudolf Jaenisch, and Sacha B. Nelson. Reduced cortical activity due to a shift in the balance between excitation and inhibition in a mouse model of rett syndrome. *Proceedings of the National Academy of Sciences of the United States of America*, 102(35):12560–12565, 2005.
- [8] Katsuhiko Tabuchi, Jacqueline Blundell, Mark R. Etherton, Robert E. Hammer, Xinran Liu, Craig M. Powell, and Thomas C. Südhof. A neuroigin-3 mutation implicated in autism increases inhibitory synaptic transmission in mice. *Science*, 318(5847):71–76, 2007.
- [9] Chris M. Woodard, Brian A. Campos, Sheng-Han Kuo, Melissa J. Nirenberg, Michael W. Nestor, Matthew Zimmer, Eugene V. Mosharov, David Sulzer, Hongyan Zhou, Daniel Paull, Lorraine Clark, Eric E. Schadt, Sergio Pablo Sardi, Lee Rubin, Kevin Eggan, Mathew Brock, Scott Lipnick, Mahendra Rao, Stephen Chang, Aiqun Li, and Scott A. Noggle. iPSC-derived dopamine neurons reveal differences between monozygotic twins discordant for parkinson’s disease. *Cell Reports*, 9(4):1173–1182, 2014.
- [10] Hayder Amin, Thierry Nieuw, Davide Lonardoni, Alessandro Maccione, and Luca Berdondini. High-resolution bioelectrical imaging of  $\alpha\beta$ -induced network dysfunction on CMOS-MEAs for neurotoxicity and rescue studies. *Scientific Reports*, 7(1):2460, 2017.

- [11] Ricardo Pineda, Christine E. Beattie, and Charles W. Hall. Closed-loop neural stimulation for pentylenetetrazole-induced seizures in zebrafish. *Disease Models & Mechanisms*, 6(1):64–71, 2013.
- [12] Alireza Gharabaghi, Dominic Kraus, Maria Teresa Leao, Martin Spüler, Armin Walter, Martin Bogdan, Wolfgang Rosenstiel, Georgios Naros, and Ulf Ziemann. Coupling brain-machine interfaces with cortical stimulation for brain-state dependent stimulation: enhancing motor cortex excitability for neurorehabilitation. *Frontiers in Human Neuroscience*, 8, 2014.
- [13] Daniel A. Wagenaar, Radhika Madhavan, Jerome Pine, and Steve M. Potter. Controlling bursting in cortical cultures with closed-loop multi-electrode stimulation. *Journal of Neuroscience*, 25(3):680–688, 2005.
- [14] Wei-Ming Chen, Herming Chiueh, Tsan-Jieh Chen, Chia-Lun Ho, Chi Jeng, Ming-Dou Ker, Chun-Yu Lin, Ya-Chun Huang, Chia-Wei Chou, Tsun-Yuan Fan, et al. A fully integrated 8-channel closed-loop neural-prosthetic cmos soc for real-time epileptic seizure control. *IEEE journal of solid-state circuits*, 49(1):232–247, 2014.
- [15] Boris Rosin, Maya Slovik, Rea Mitelman, Michal Rivlin-Etzion, Suzanne N. Haber, Zvi Israel, Eilon Vaadia, and Hagai Bergman. Closed-loop deep brain stimulation is superior in ameliorating parkinsonism. *Neuron*, 72(2):370–384, 2011.
- [16] Alfred Stett, Ulrich Egert, Elke Guenther, Frank Hofmann, Thomas Meyer, Wilfried Nisch, and Hugo Haemmerle. Biological application of microelectrode arrays in drug discovery and basic research. *Analytical and Bioanalytical Chemistry*, 377(3):486–495, 2003.
- [17] Franke F, Jäckel D, Dragas J, Müller J, Radivojevic M, Bakkum D, and Hierlemann A. High-density microelectrode array recordings and real-time spike sorting for closed-loop experiments: an emerging technology to study neural plasticity. *Frontiers in neural circuits*, 6:105–105, 2012.
- [18] Marie Engelen J. Obien, Kosmas Deligkaris, Torsten Bullmann, Douglas J. Bakkum, and Urs Frey. Revealing neuronal function through microelectrode array recordings. *Frontiers in Neuroscience*, 8, 2015.
- [19] Mikhail A. Lebedev and Miguel A. L. Nicolelis. Brain-machine interfaces: past, present and future. *Trends in Neurosciences*, 29(9):536–546, 2006.
- [20] Mikhail A. Lebedev and Miguel A. L. Nicolelis. Brain-machine interfaces: From basic science to neuroprostheses and neurorehabilitation. *Physiological Reviews*, 97(2):767–837, 2017.
- [21] Jennifer L Collinger, Brian Wodlinger, John E Downey, Wei Wang, Elizabeth C Tyler-Kabara, Douglas J Weber, Angus JC McMorland, Meel Velliste, Michael L Boninger, and Andrew B Schwartz. High-performance

- neuroprosthetic control by an individual with tetraplegia. *The Lancet*, 381(9866):557–564, 2013.
- [22] Leigh R. Hochberg, Daniel Bacher, Beata Jarosiewicz, Nicolas Y. Masse, John D. Simeral, Joern Vogel, Sami Haddadin, Jie Liu, Sydney S. Cash, Patrick van der Smagt, and John P. Donoghue. Reach and grasp by people with tetraplegia using a neurally controlled robotic arm. *Nature*, 485(7398):372–375, 2012.
- [23] Jan Müller, Marco Ballini, Paolo Livi, Yihui Chen, Milos Radivojevic, Amir Shadmani, Vijay Viswam, Ian L. Jones, Michele Fiscella, Roland Diggelmann, Alexander Stettler, Urs Frey, Douglas J. Bakkum, and Andreas Hierlemann. High-resolution CMOS MEA platform to study neurons at subcellular, cellular, and network levels. *Lab on a Chip*, 15(13):2767–2780, 2015.
- [24] Marco Ballini, Jan Müller, Paolo Livi, Yihui Chen, Urs Frey, Alexander Stettler, Amir Shadmani, Vijay Viswam, Ian Lloyd Jones, David Jäckel, et al. A 1024-channel cmos microelectrode array with 26,400 electrodes for recording and stimulation of electrogenic cells in vitro. *IEEE Journal of Solid-State Circuits*, 49(11):2705–2719, 2014.
- [25] Dale Purves, George J Augustine, David Fitzpatrick, WC Hall, AS LaMantia, JO McNamara, and LE White. *Neuroscience, Fourth Edition*. Sunderland: Sinauer Associates, Inc, 2008.
- [26] Elaine Nicpon Marieb and Katja Hoehn. *Human anatomy & physiology*. Pearson Education, 2007.
- [27] Eric R Kandel, James H Schwartz, Thomas M Jessell, Steven A Siegelbaum, and A James Hudspeth. *Principles of neural science*, volume 4. McGraw-hill New York, 2000.
- [28] Matt Carter and Jennifer C. Shieh. *Guide to Research Techniques in Neuroscience*. Academic Press, 2015.
- [29] E. D. Adrian and G. Moruzzi. Impulses in the pyramidal tract. *The Journal of Physiology*, 97(2):153–199, 1939.
- [30] B. L. McNaughton, J. O’Keefe, and C. A. Barnes. The stereotrode: a new technique for simultaneous isolation of several single units in the central nervous system from multiple unit records. *Journal of Neuroscience Methods*, 8(4):391–397, 1983.
- [31] Matthew A Wilson and Bruce L McNaughton. Dynamics of the hippocampal ensemble code for space. *Science*, 261(5124):1055–1058, 1993.
- [32] John O’Keefe and Michael L. Recce. Phase relationship between hippocampal place units and the EEG theta rhythm. *Hippocampus*, 3(3):317–330, 1993.

- [33] M. Kuperstein and H. Eichenbaum. Unit activity, evoked potentials and slow waves in the rat hippocampus and olfactory bulb recorded with a 24-channel microelectrode. *Neuroscience*, 15(3):703–712, 1985.
- [34] Ian H. Stevenson and Konrad P. Kording. How advances in neural recording affect data analysis. *Nature Neuroscience*, 14(2):139–142, 2011.
- [35] Miguel A. L. Nicolelis, Dragan Dimitrov, Jose M. Carmena, Roy Crist, Gary Lehew, Jerald D. Kralik, and Steven P. Wise. Chronic, multisite, multielectrode recordings in macaque monkeys. *Proceedings of the National Academy of Sciences*, 100(19):11041–11046, 2003.
- [36] J. K. Chapin, K. A. Moxon, R. S. Markowitz, and M. A. Nicolelis. Real-time control of a robot arm using simultaneously recorded neurons in the motor cortex. *Nature Neuroscience*, 2(7):664–670, 1999.
- [37] Johnson Md, Franklin Rk, Gibson Md, Brown Rb, and Kipke Dr. Implantable microelectrode arrays for simultaneous electrophysiological and neurochemical recordings., implantable microelectrode arrays for simultaneous electrophysiological and neurochemical recordings. *Journal of neuroscience methods*, *Journal of neuroscience methods*, 174, 174(1):62, 62–70, 2008.
- [38] Jonathan Viveri, Dae-Hyeong Kim, Leif Vigeland, Eric S. Frechette, Justin A. Blanco, Yun-Soung Kim, Andrew E. Avrin, Vineet R. Tiruvadi, Suk-Won Hwang, Ann C. Vanleer, Drausin F. Wulsin, Kathryn Davis, Casey E. Gelber, Larry Palmer, Jan Van der Spiegel, Jian Wu, Jianliang Xiao, Yonggang Huang, Diego Contreras, John A. Rogers, and Brian Litt. Flexible, foldable, actively multiplexed, high-density electrode array for mapping brain activity in vivo. *Nature Neuroscience*, 14(12):1599–1605, 2011.
- [39] Chiayu Chiu and Michael Weliky. Spontaneous activity in developing ferret visual cortex in vivo. *Journal of Neuroscience*, 21(22):8906–8914, 2001.
- [40] Yasuhiko Jimbo and Akio Kawana. Electrical stimulation and recording from cultured neurons using a planar electrode array. *Bioelectrochemistry and Bioenergetics*, 29(2):193–204, 1992.
- [41] Xiangning Li, Wei Zhou, Shaoqun Zeng, Man Liu, and Qingming Luo. Long-term recording on multi-electrode array reveals degraded inhibitory connection in neuronal network development. *Biosensors and Bioelectronics*, 22(7):1538–1543, 2007.
- [42] Wei Gong, Jure Senčar, Douglas J. Bakkum, David Jäckel, Marie Engelen J. Obien, Milos Radivojevic, and Andreas R. Hierlemann. Multiple single-unit long-term tracking on organotypic hippocampal slices using high-density microelectrode arrays. *Frontiers in Neuroscience*, 10, 2016.

- [43] M. Gandolfo, A. Maccione, M. Tedesco, S. Martinoia, and L. Berdondini. Tracking burst patterns in hippocampal cultures with high-density CMOS-MEAs. *Journal of Neural Engineering*, 7(5):056001, 2010.
- [44] Douglas J. Bakkum, Urs Frey, Milos Radivojevic, Thomas L. Russell, Jan Müller, Michele Fiscella, Hirokazu Takahashi, and Andreas Hierlemann. Tracking axonal action potential propagation on a high-density microelectrode array across hundreds of sites. *Nature Communications*, 4:ncomms3181, 2013.
- [45] Ellese Cotterill, Diana Hall, Kathleen Wallace, William R. Mundy, Stephen J. Eglén, and Timothy J. Shafer. Characterization of early cortical neural network development in multiwell microelectrode array plates. *Journal of Biomolecular Screening*, 21(5):510–519, 2016.
- [46] Andreas Hierlemann, Urs Frey, Sadik Hafizovic, and Flavio Heer. Growing cells atop microelectronic chips: interfacing electrogenic cells in vitro with cmos-based microelectrode arrays. *Proceedings of the IEEE*, 99(2):252–284, 2011.
- [47] Urs Frey, Jan Sedivy, Flavio Heer, Rene Pedron, Marco Ballini, Jan Mueller, Douglas Bakkum, Sadik Hafizovic, Francesca D Faraci, Frauke Greve, et al. Switch-matrix-based high-density microelectrode array in cmos technology. *IEEE Journal of Solid-State Circuits*, 45(2):467–482, 2010.
- [48] Luca Berdondini, Kilian Imfeld, Alessandro Maccione, Mariateresa Tedesco, Simon Neukom, Milena Koudelka-Hep, and Sergio Martinoia. Active pixel sensor array for high spatio-temporal resolution electrophysiological recordings from single cell to large scale neuronal networks. *Lab on a Chip*, 9(18):2644–2651, 2009.
- [49] X Yuan, S Kim, J Juyon, M D’Urbino, T Bullmann, Y Chen, Alexander Stettler, Andreas Hierlemann, and Urs Frey. A microelectrode array with 8,640 electrodes enabling simultaneous full-frame readout at 6.5 kfps and 112-channel switch-matrix readout at 20 ks/s. In *VLSI Circuits (VLSI-Circuits), 2016 IEEE Symposium on*, pages 1–2. IEEE, 2016.
- [50] Ben Johnson, Shane T Peace, Albert Wang, Thomas A Cleland, and Alyosha Molnar. A 768-channel cmos microelectrode array with angle sensitive pixels for neuronal recording. *IEEE Sensors Journal*, 13(9):3211–3218, 2013.
- [51] György Buzsáki. Large-scale recording of neuronal ensembles. *Nature Neuroscience*, 7(5):446–451, 2004.
- [52] Michael S. Lewicki. A review of methods for spike sorting: the detection and classification of neural action potentials. *Network: Computation in Neural Systems*, 9(4):R53–R78, 1998.



- [53] M. Chiappalone, A. Novellino, I. Vajda, A. Vato, S. Martinoia, and J. van Pelt. Burst detection algorithms for the analysis of spatio-temporal patterns in cortical networks of neurons. *Neurocomputing*, 65-66:653–662, 2005.
- [54] V Pasquale, P Massobrio, LL Bologna, M Chiappalone, and S Martinoia. Self-organization and neuronal avalanches in networks of dissociated cortical neurons. *Neuroscience*, 153(4):1354–1369, 2008.
- [55] Catherine S. Cutts and Stephen J. Eglén. Detecting pairwise correlations in spike trains: An objective comparison of methods and application to the study of retinal waves. *Journal of Neuroscience*, 34(43):14288–14303, 2014.
- [56] Pierre Yger, Giulia L. B. Spampinato, Elric Esposito, Baptiste Lefebvre, Stephane Deny, Christophe Gardella, Marcel Stimberg, Florian Jetter, Guenther Zeck, Serge Picaud, Jens Duebel, and Olivier Marre. Fast and accurate spike sorting in vitro and in vivo for up to thousands of electrodes. *bioRxiv*, page 067843, 2016.
- [57] Felix Franke, Rodrigo Quián Quiroga, Andreas Hierlemann, and Klaus Obermayer. Bayes optimal template matching for spike sorting - combining fisher discriminant analysis with optimal filtering. *Journal of Computational Neuroscience*, 38(3):439–459, 2015.
- [58] Yuning Yang and Andrew J Mason. On-chip spike clustering & classification using self organizing map for neural recording implants. In *Biomedical Circuits and Systems Conference (BioCAS), 2011 IEEE*, pages 145–148. IEEE, 2011.
- [59] Gopal Santhanam, Maneesh Sahani, Stephen I Ryu, and Krishna V Shenoy. An extensible infrastructure for fully automated spike sorting during on-line experiments. In *Engineering in Medicine and Biology Society, 2004. IEMBS'04. 26th Annual International Conference of the IEEE*, volume 2, pages 4380–4384. IEEE, 2004.
- [60] Douglas J Bakkum, Milos Radivojevic, Urs Frey, Felix Franke, Andreas Hierlemann, and Hirokazu Takahashi. Parameters for burst detection. *Frontiers in computational neuroscience*, 7, 2013.
- [61] Lin Chen, Yong Deng, Weihua Luo, Zhen Wang, and Shaoqun Zeng. Detection of bursts in neuronal spike trains by the mean inter-spike interval method. *Progress in Natural Science*, 19(2):229–235, 2009.
- [62] J Van Pelt, PS Wolters, WLC Rutten, MA Corner, P Van Hulten, and GJA Ramakers. Spatio-temporal firing in growing networks cultured on multi-electrode arrays. *Proc. World Congr. Neuroinformatics, Rattay F (ed) Argesim Report*, (20):462–467, 2001.
- [63] David R Brillinger. Measuring the association of point processes: a case history. *The American Mathematical Monthly*, 83(1):16–22, 1976.

- [64] Shinya Ito, Michael E Hansen, Randy Heiland, Andrew Lumsdaine, Alan M Litke, and John M Beggs. Extending transfer entropy improves identification of effective connectivity in a spiking cortical network model. *PloS one*, 6(11):e27431, 2011.
- [65] Matteo Garofalo, Thierry Nieu, Paolo Massobrio, and Sergio Martinoia. Evaluation of the performance of information theory-based methods and cross-correlation to estimate the functional connectivity in cortical networks. *PLOS ONE*, 4(8):e6482, 2009.
- [66] Milos Radivojevic, David Jäckel, Michael Altermatt, Jan Müller, Vijay Viswam, Andreas Hierlemann, and Douglas J. Bakkum. Electrical identification and selective microstimulation of neuronal compartments based on features of extracellular action potentials. *Scientific Reports*, 6, 2016.
- [67] Julia H. Downes, Mark W. Hammond, Dimitris Xydas, Matthew C. Spencer, Victor M. Becerra, Kevin Warwick, Ben J. Whalley, and Slawomir J. Nasuto. Emergence of a small-world functional network in cultured neurons. *PLOS Computational Biology*, 8(5):e1002522, 2012.
- [68] Mark R. Dranias, Han Ju, Ezhilarasan Rajaram, and Antonius M. J. Van Dongen. Short-term memory in networks of dissociated cortical neurons. *Journal of Neuroscience*, 33(5):1940–1953, 2013.
- [69] Partha Mitra. *Observed brain dynamics*. Oxford University Press, 2007.
- [70] Daniel N Hill, Samar B Mehta, and David Kleinfeld. Quality metrics to accompany spike sorting of extracellular signals. *Journal of Neuroscience*, 31(24):8699–8705, 2011.
- [71] Daniel N Hill, Samar B Mehta, and David Kleinfeld. Ultramegasort 2000 manual. 2012.
- [72] Gaute T Einevoll, Felix Franke, Espen Hagen, Christophe Pouzat, and Kenneth D Harris. Towards reliable spike-train recordings from thousands of neurons with multielectrodes. *Current opinion in neurobiology*, 22(1):11–17, 2012.
- [73] Edward M Schmidt. Computer separation of multi-unit neuroelectric data: a review. *Journal of neuroscience methods*, 12(2):95–111, 1984.
- [74] Christopher M Bishop. *Pattern recognition and machine learning*. Springer, 2006.
- [75] Roland Diggelmann, Michele Fiscella, Antonia Drinnenberg, Felix Franke, Botond Roska, and Andreas Hierlemann. Using high-density meas for high-throughput retinal ganglion cell type classification. In *Front. Neurosci. Conference Abstract: MEA Meeting*, 2016.

- [76] Roland Diggelmann, Michele Fiscella, Andreas Hierlemann, and Felix Franke. Fully automatic spike-sorting algorithm for high-density multi-electrode arrays. In press.
- [77] Christophe Pouzat, Ofer Mazor, and Gilles Laurent. Using noise signature to optimize spike-sorting and to assess neuronal classification quality. *Journal of neuroscience methods*, 122(1):43–57, 2002.
- [78] Keinosuke Fukunaga and Larry Hostetler. The estimation of the gradient of a density function, with applications in pattern recognition. *IEEE Transactions on information theory*, 21(1):32–40, 1975.
- [79] Patrick E McKnight and Julius Najab. Mann-Whitney U Test. *Corsini Encyclopedia of Psychology*, 2010.
- [80] Peter Dayan and Laurence F Abbott. *Theoretical neuroscience*, volume 806. Cambridge, MA: MIT Press, 2001.
- [81] Mikail Rubinov and Olaf Sporns. Complex network measures of brain connectivity: Uses and interpretations. *NeuroImage*, 52(3):1059–1069, 2010.
- [82] Tom Preston-Werner, Chris Wanstrath, and PJ Hyett. GitHub git repository hosting service, 2008.
- [83] Radhika Madhavan, Zenas C Chao, Daniel A Wagenaar, Douglas J Bakkum, and Steve M Potter. Multi-site stimulation quiets network-wide spontaneous bursts and enhances functional plasticity in cultured cortical networks. In *Engineering in Medicine and Biology Society, 2006. EMBS'06. 28th Annual International Conference of the IEEE*, pages 1593–1596. IEEE, 2006.